NEUTRON SCATTERING STUDIES OF CRUDE OIL VISCOSITY REDUCTION WITH ELECTRIC FIELD

A Dissertation
Submitted to
the Temple University Graduate Board

In Partial Fulfillment
of the Requirements for the Degree
DOCTOR OF PHILOSOPHY

---

by
Enpeng Du
July, 2015

Examining Committee Members:

Rongjia Tao, Advisory Chair, Physics
Ted Burkhardt, Physics
Xifan Wu, Physics
Jim Chen, Engineering
Judy Zhang, Engineering

ABSTRACT

NEUTRON SCATTERING STUDIES OF CRUDE OIL VISCOSITY REDUCTION WITH ELECTRIC FIELD

Enpeng Du

Doctor of Philosophy

Temple University, 2015

Doctoral Advisory Committee Chair: Dr. Rongjia Tao

Small-angle neutron scattering (SANS) is a very powerful laboratory technique for micro structure research which is similar to the small angle X-ray scattering (SAXS) and light scattering for microstructure investigations in various materials. In small-angle neutron scattering (SANS) technique, the neutrons are elastically scattered by changes of refractive index on a nanometer scale inside the sample through the interaction with the nuclei of the atoms present in the sample. Because the nuclei of all atoms are compact and of comparable size, neutrons are capable of interacting strongly with all atoms. This is in contrast to X-ray techniques where the X-rays interact weakly with hydrogen, the most abundant element in most samples. The SANS refractive index is directly related to the scattering length density and is a measure of the strength of the interaction of a neutron wave with a given nucleus. It can probe inhomogeneities in the nanometer scale from 1nm to 1000nm. Since the SANS technique probes the length scale in a very useful range, this technique provides valuable information over a wide variety of scientific and

technological applications, including chemical aggregation, defects in materials, surfactants, colloids, ferromagnetic correlations in magnetism, alloy segregation, polymers, proteins, biological membranes, viruses, ribosome and macromolecules. Quoting the Nobel committee, when awarding the prize to C. Shull and B. Brockhouse in 1994: "Neutrons tell you where the atoms are and what the atoms do". At NIST, there is a single beam of neutrons generated from either reactor or pulsed neutron source and selected by velocity selector. The beam passes through a neutron guide then scattered by the sample. After the sample chamber, there are 2D gas detectors to collect the elastic scattering information. SANS usually uses collimation of the neutron beam to determine the scattering angle of a neutron, which results in an even lower signal-to-noise ratio for data that contains information on the properties of a sample. We can analyze the data acquisition from the detectors and get the information on size, shape, etc. This is why we choose SANS as our research tool.

The world's top energy problems are security concerns, climate concerns and environmental concerns. So far, oil (37%) is still the No.1 fuel in world energy consumption (Oil 37%, Coal 25%, Bio-fuels 0.2%, Gas 23%, Nuclear 6%, Biomass 4%, Hydro 3%, Solar heat 0.5%, Wind 0.3%, Geothermal 0.2% and Solar photovoltaic 0.04%). Even more and more alternative energy: bio-fuels, nuclear and solar energy will be used in the future, but nuclear energy has a major safety issue after the Japanese Fukushima I nuclear accidents, and other energies contribute only a small percent. Thus, it is very important to improve the efficiency and reduce the population of petroleum products.

There is probably one thing that we can all agree on: the world's energy reserves are not unlimited. Even though it is limited, only 30% of the oil reserves is conventional oil, so in order to produce, transport, and refine of heavy crude oil without wasting huge amounts of energy, we need to reduce the viscosity without using high temperature stream heating or diluent; As more and more off-shore oil is exploited at that we need reduce the viscosity without increasing temperature.

The whole petroleum consumed in U.S. in 2009 was 18.7 million barrels per day and 35% of all the energy we consumed. Diesel is one of the very important fossil fuel which is about 20% of petroleum consumed. Most of the world's oils are non-conventional, 15 % of heavy oil, 25 % of extra heavy oil, 30 % of the oil sands and bitumen, and the conventional oil reserves is only 30%. The oil sand is closely related to the heavy crude oil, the main difference being that oil sands generally do not flow at all. For efficient energy production and conservation, how to lower the liquated fuel and crude oil viscosity is a very important topic. Dr. Tao with his group at Temple University, using his electro or magnetic rheological viscosity theory has developed a new technology, which utilizes electric or magnetic fields to change the rheology of complex fluids to reduce the viscosity, while keeping the temperature unchanged. After we successfully reduced the viscosity of crude oil with field and investigated the microstructure changing in various crude oil samples with SANS, we have continued to reduce the viscosity of heavy crude oil, bunker diesel, ultra low sulfur diesel, bio-diesel and crude oil and ultra low temperature with electric field treatment.

Our research group developed the viscosity electrorheology theory and investigated flow rate with laboratory and field pipeline. But we never visualize this aggregation. The

small angle neutron scattering experiment has confirmed the theoretical prediction that a strong electric field induces the suspended nano-particles inside crude oil to aggregate into short chains along the field direction. This aggregation breaks the symmetry, making the viscosity anisotropic: along the field direction, the viscosity is significantly reduced. The experiment enables us to determine the induced chain size and shape, verifies that the electric field works for all kinds of crude oils, paraffin-based, asphalt-based, and mix-based. The basic physics of such field induced viscosity reduction is applicable to all kinds of suspensions.

ACKNOWLEDGMENTS

I would like to greatly thank my advisor, Dr. Rongjia Tao, for all his encouragement, help and constant support throughout my graduate career at Physics Department of Temple University and at other institutes. He gives me plenty of free space to develop my research on ER fluids, energy saving, neutron scattering, iron detector to Geant4 simulation. He strongly supported me to attend the NIST neutron science summer school, University Pennsylvania geant4 summer school and to apply for beam time at NIST. Also he supports me to work in Japan and China. Without his support, I would not have been able to complete this work. I greatly value his enthusiasm for his work and love for his students. He is a brilliant physicist from whom I can always get inspiration and knowledge, as well as a friend on whom I can count to overcome difficulties.

I would also like to thanks Dr. Yun Liu from NIST. He offered us his research beam time for our test, helped us to pass the safe check and scheduled the test. He also gave us a following up talk to introduce SANS at Temple University.

I would also like to thank Dr. Boualem Hammouda from NIST and my fellow group members Dr. Xiaojun Xu, Dr. Hong Tang and Dr. Ke Huang for sharing their invaluable scientific knowledge and experimental expertise. The training they gave me was immensely helpful, and I am extremely grateful to them for the many hours they spent explaining concepts and helping me in the lab.

Thank you, Dr. Marjatta Lyyra, for helping me to enroll in the Physics Department at Temple University and reunite with my family so I could focus on

research.

I would like to thank my committee members, Dr. Theodore W. Burkhardt, Dr. Xifan Wu, Dr. Jim Chen, Dr. Judy Zhang, for their advice and kind support of my study and research work during my years in Temple University, as well as their efforts in reviewing the thesis for me.

Thank you also to Ed Kaczanowicz and Matthew McCormick for their mechanical assistance, and to Richard J. Harris for his help in our electrical problems, and to David W. Plasket for his help about house build quartz cell. Their indispensable technical support was greatly appreciated.

I must also acknowledge Dr. Peter S. Riseborough and Dr. Tan Yuan and Dr. Andreas Metz, Dr. Chyan Long Lin for their suggestions about my research and for the time they spent attending my progressive reports throughout my graduate program.

Thank you also to Dr. John Noel and Mr. John Noel for their help in all teaching matters, large and small.

Appreciation also goes out to Constance O'Donnell, Karen E. Woods-Wilson and Jacqueline Farley of the Department of Physics administration office staff for all the instances in which their assistance helped me along the way.

This work utilized facilities supported in part by the National Science Foundation under Agreement No. DMR-0944772.

We acknowledge the support of the National Institute of Standards and Technology, U.S. Department of Commerce, in providing the neutron research facilities used in this work.

I also thank my family: mom Changcun Qu and mother in law Mingrong Wang,

father in law Mingde Guan and brother in law Junsheng Guan, for their love, strongly support, knowledge, and insight shared in phone conversations over these last few years. The largest thanks must go to my wife, Yafei Guan, for loving me these past eight years during both the easy and hard times and loving our kids.

Dedicated to my wife Yafei and my cute/lovely son William Pengfei Du and my adorable daughter Grace Pengya Du.

Dedicated to my wife yafei
and my son and my daughter
for the glory of God

TABLE OF CONTENTS

LIST OF FIGURES

Figure Page

LIST OF TABLES

CHAPTER 1

DR. TAO`S RHEOLOGY THEORY

1.1 Viscosity

The viscosity of a fluid is a measure of its resistance to gradual deformation by shear stress or tensile stress. For liquids, it corresponds to the informal concept of "stickiness". For example, honey has a much higher viscosity than water.

Viscosity is a property arising from collisions between neighboring particles in a fluid that are moving at different velocities. When the fluid is forced through a tube, the particles which comprise the fluid generally move more quickly near the tube's axis and more slowly near its walls; therefore some stress, (such as a pressure difference between the two ends of the tube), is needed to overcome the friction between particle layers to keep the fluid moving. For the same velocity pattern, the stress required is proportional to the fluid's viscosity.

Viscosity coefficients can by classified as dynamic viscosity, kinematic viscosity, volume viscosity, shear viscosity, and extensional viscosity, depending on the nature of applied stress and nature of the fluid. For my research, these are limited to dynamic viscosity and kinematic viscosity. [1] [2] [3]

1.1.1 Dynamic Viscosity

The dynamic or absolute coefficient of viscosity is a measure of internal resistance. Dynamic viscosity is the tangential force per unit area required to move one horizontal plane with respect to another plane at an unit velocity when maintaining an unit distance apart in the fluid[1] [3] [4] [5].

The shearing stress between the layers of a none turbulent fluid moving in straight parallel lines can be defined in terms of Fig. 1.1

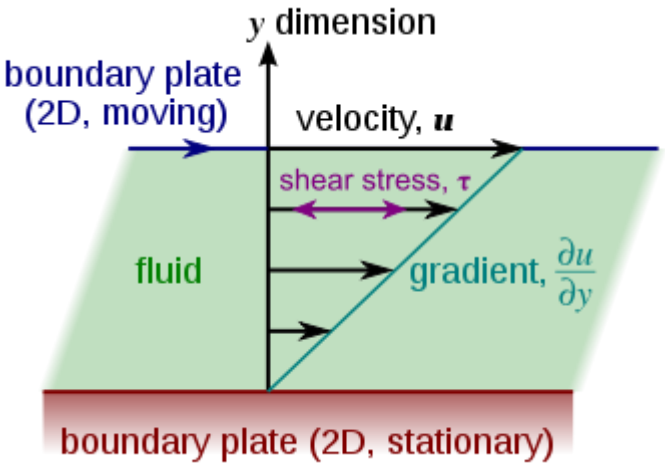

Figure 1.1 Laminar shear of fluid between two plates. [4] [5]

If the speed of the top plate is small enough, the fluid particles will move parallel to it, and their speed will vary linearly from zero at the bottom to u at the top. Each layer of fluid will move faster than the one just below it, and friction between them will give rise to a force resisting their relative motion. In particular, the fluid will apply on the top plate a force in the direction opposite to its motion, and an equal but opposite one to the bottom plate. An external force is therefore required in order to keep the top plate moving at constant speed. [4] [5]

The magnitude F of this force is found to be proportional to the speed u and the area A of each plate, and inversely proportional to their separation y:

$$F = \mu A \frac{u}{y} \tag{1.1}$$

The proportionality factor μ in this formula is the viscosity (specifically, the dynamic viscosity) of the fluid.

The ratio $\frac{\partial u}{\partial y}$ is called the rate of shear deformation or shear velocity, and is the derivative of the fluid speed in the direction perpendicular to the plates. Isaac Newton expressed the viscous forces in terms of derivatives of the flow velocity.[4] [5]

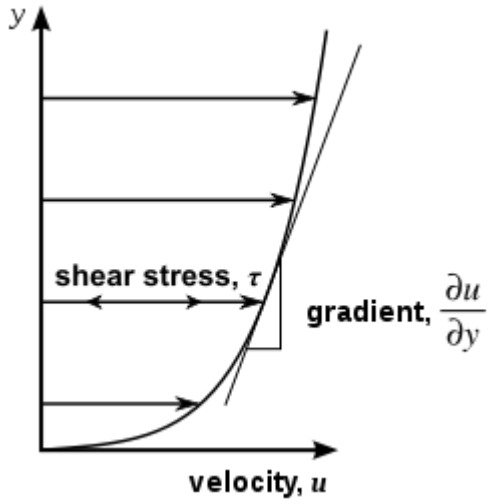

Figure 1.2 In a general parallel flow (such as could occur in a straight pipe), the shear stress is proportional to the gradient of the velocity.[4] [5]

The dynamic viscosity can be expressed

$$\tau = \mu \frac{\partial u}{\partial y} \tag{1.2}$$

where $\tau = \frac{F}{A}$ and $\frac{\partial u}{\partial y}$ is the local shear velocity. This formula assumes that the flow is moving along parallel lines and the y axis, perpendicular to the flow, points in the

direction of maximum shear velocity. This equation can be used where the velocity does not vary linearly with y, such as in fluid flowing through a pipe.

τ = shearing stress (N/m^2)

μ = dynamic viscosity ($N\ s/m^2$)

$\frac{\partial u}{\partial y}$ velocity (m/s) changing per unit distance between layers (m)

Equation (1.2) is known as the Newton`s Law of Friction.

The SI unit of dynamic viscosity is pascal-second, or $Pa \cdot s$, which equals to $kg \cdot m^{-1} \cdot s^{-1}$. The dynamic viscosity is also often expressed in CGS (centimeter-gram-second) unit as Poise, or P, which equals to $g / cm \cdot s$, or $1/10\ Pa \cdot s$. Since P is a quite large unit, instead centiPoise, or cP, is used more frequently, where $1\ P = 100\ cP$. Water at 20.2°C has an dynamic viscosity of $1\ cP$.[4]

1.1.2 Kinematic Viscosity

In some cases, people are more interested in the ratio of the viscous force to the inertial force. The viscous force is characterized by dynamic viscosity η and the inertial force is characterized by fluid density ρ. This ratio is called the kinematic viscosity υ, which is obtained by dividing the absolute viscosity of a fluid with it's mass density

$$\nu = \frac{\eta}{\rho} \tag{1.3}$$

υ has a SI unit of Stoke (St), where $1\ St = 10^{-4}\ m^2 / s$. Similar to Poise, since the Stoke is an impractically large unit, it is usually divided by 100 to give the unit called Centistokes (cSt) where $St = 100\ cSt$.[3] [4]

1.1.3 Reduce Viscosity Is Very Important

Flows through pipes and channels are the most common and important way of transporting fluids. To enhance the flow output via pipeline requires reducing the fluid viscosity. These issues are not only crucial for many industrial and engineer applications, but also important in basic science [21-24][30-33]. Unfortunately, no method is currently available to reduce the fluid viscosity and in pipeline simultaneously and effectively.

Pipeline transport is the transportation of goods or material through a pipe. The best data, in 2014, gives a total of slightly less than 3.5 million km of pipeline in 120 countries of the world.[25] [26] The United States had 65%, Russia had 8%, and Canada had 3%. Thus 75% of all pipeline transport was in three countries.[25] [26] Pipelines are generally the most economical way to transport large quantities of oil, refined oil products or natural gas over land. In order to transport crude oil through a pipeline, we need both pump station and heat stations to overcome the crude oil viscosity. Even with these, if the viscosity is bigger than 350 centistokes, pipeline transport is difficult. As seasonal temperatures vary, the blends of heavier crude oils with diluent are changed to meet the viscosity limit. How to reduce viscosity is very important and can affect energy saving.

1.2 **Viscosity and Volume Fraction of Liquid Suspension** [5] [6][1]

Einstein derived an equation describing the relationship of the viscosity η of a dilute liquid suspension of non-interacting uniform spheres and the viscosity of the base liquid η_0. Einstein showed that the apparent viscosity η is given by

$$\eta = \eta_0(1 + 2.5\phi) \tag{1.4}$$

where η_0 is the viscosity of the base liquid and ϕ is the volume fraction of the non-interacting uniform spheres. This is known as Einstein's law of viscosity [6]. It is restricted to very dilute systems with volume fraction $\phi < 0.03$ [7]. Many approaches have been tried to extend Einstein's equation for higher volume fraction by incorporating the correction term $b\phi^2$ to the equation, where b is the coefficient for ϕ^2. The updated equation takes the form

$$\eta = \eta_0(1 + 2.5\phi + b\phi^2) \tag{1.5}$$

Several theoretical values that have been obtained from different models for b, 14.1, 12.6 and 7.35. [8] Now the generally accepted value for b is 6.2, but equation (1.4) only holds for liquid suspensions with slightly higher volume fraction. [10] At still higher volume fractions, η increases even more steeply than what is predicted by equation (1.5), and a new approach has to be developed.

Mooney proposed an equation for higher volume fraction [11] and Krieger and Dougherty developed it [12] and solved the problem very well. Suppose a certain amount of small spheres is added to the solvent. The change of viscosity $d\eta$ is caused by adding the volume fraction $d\phi$ of particles into a suspension, which already has volume fraction of ϕ and viscosity $\eta(\phi)$.

Adding the same amount of spheres, to suspensions of different volume fraction apparently has a different impact on the viscosity. The change in the viscosity of a dilute suspension caused by adding $d\phi$ particles is much smaller than that of a suspension of high volume fraction. In liquid suspensions, there is a maximum volume faction ϕ_m available for adding particles. Since it is a random packing, ϕ_m is about 0.64, the maximum value for random packing. [13]

Keeping that in mind, when we add $d\phi$ volume fraction of spheres to a liquid suspension of volume fraction ϕ, the net available volume fraction to add the spheres is

$$1 - \frac{\phi}{\phi_m} \tag{1.6}$$

Therefore, from the Einstein formula,

$$d\eta = 2.5\eta \frac{d\phi}{(1-\frac{\phi}{\phi_m})} \tag{1.7}$$

or

$$\frac{d\eta}{\eta} = 2.5 \frac{d\phi}{(1-\frac{\phi}{\phi_m})} \tag{1.8}$$

Using $\eta = \eta_0$ at $\phi = 0$, equation 1.7 can be integrated. Hence the viscosity of liquid suspension of spheres at high volume fraction is given by

$$\frac{\eta}{\eta_0} = (1 - \frac{\phi}{\phi_m})^{-2.5\phi_m} \tag{1.9}$$

or

$$\eta_r = (1 - \frac{\phi}{\phi_m})^{-2.5\phi_m} \tag{1.10}$$

Here $\eta_r = \frac{\eta}{\eta_0}$ is the relative viscosity.

This formula equation 1.13 is accurate only if the volume fraction of the spheres $\phi < 0.01$. [7]

For high ϕ, i.e $\phi \geq 0.01$, the maximum volume fraction, ϕ_m must be considered to be available for adding particles. Krieger-Dougherty introduced the intrinsic viscosity, with $[\eta]$ instead of 2.5, which is only good for uniform spheres, [12,133], replacing equation (1.10) by

$$\frac{\eta}{\eta_0} = (1 - \frac{\phi}{\phi_m})^{-[\eta]\phi_m} \qquad (1.11)$$

According to the Krieger-Dougherty formula, there are two ways to reduce the viscosity: 1) Raise the temperature to reduce η_0, requiring much energy; 2) Change the micro-structure, to increase ϕ_m and reduce η. The effective viscosity depends on how much dissipation of energy there is between the suspended particles and the base liquid. High ϕ_m indicates more freedom for the suspended particles and therefore, lower viscosity. Without raising the temperature, there are three mechanisms to reduce the viscosity of liquid suspensions: 1) Increase the size of the suspended particles; 2) Increase the polydispersity; 3) Make the shape of particles more favorable for flow. [30-33]

First, viscosity is reduced if the suspended particle size increases. Monodisperse suspensions: As the particle size increases, η is reduced [Fig. 1.1, 1.2].

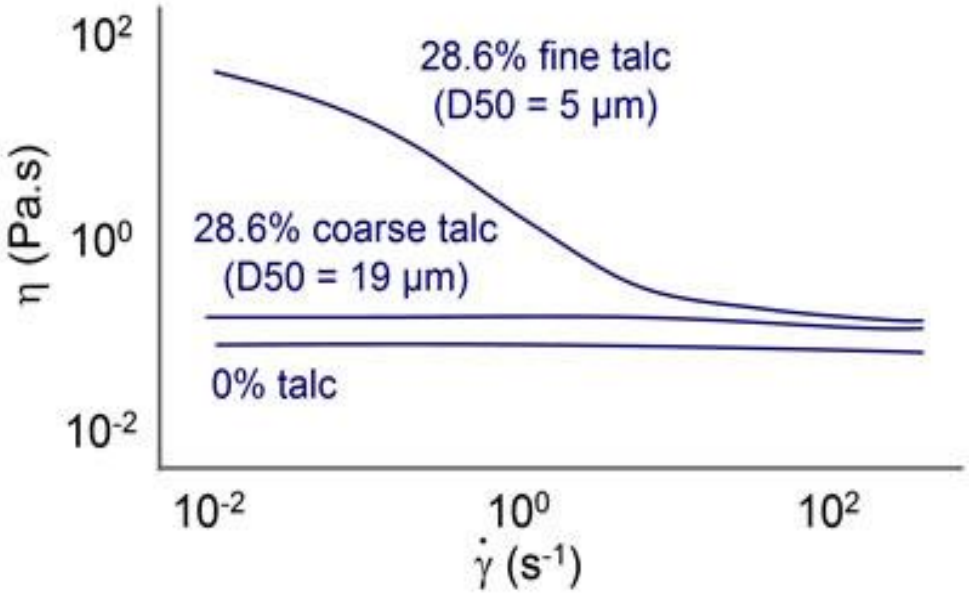

Fig 1,3. A Plots adapted from "making the connection - particle size, size distribution and rheology", Fletcher & Hill, adapted with kind permission. Particle Size Affects Viscosity at Same Volume Percentage (Slightly Larger Particle Diameters). Diagram shows viscosity versus shear rate for base liquid and mono-dispersion systems with particle diameters of 5 μm and 19 μm. The base liquid is Newtonian and the system with 28.6% coarse talc is still Newtonian, whereas the system with 28.6% fine talc has much higher viscosity at low shear rate and becomes non-Newtonian. Note. From Making the connection - particle size, size distribution and rheology. [9]

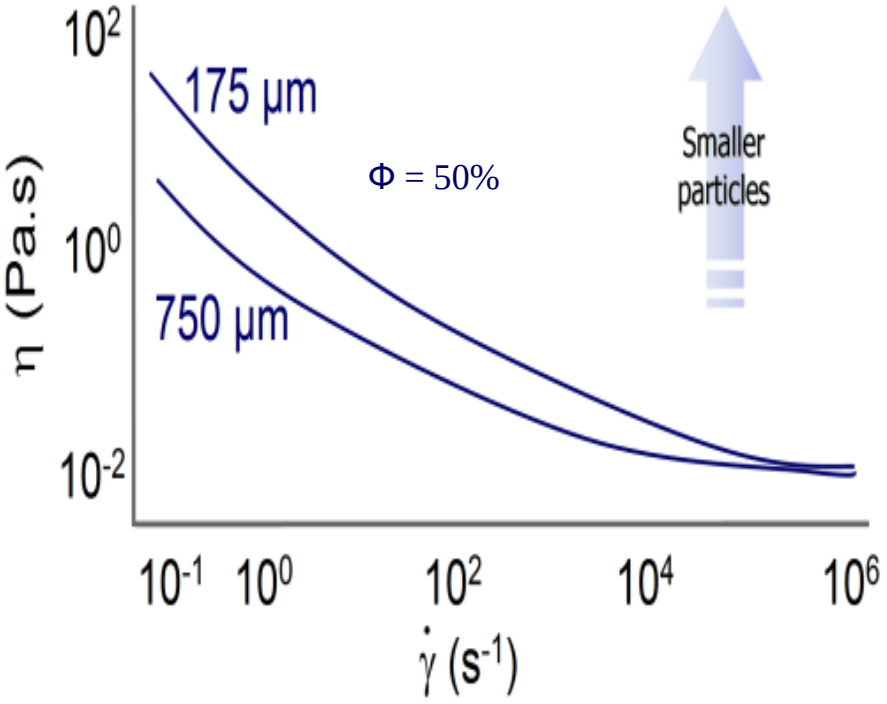

Fig 1,3. B Particle Size Affects Viscosity at Same Volume Percentage (Much Larger Particle Diameters). Diagram shows viscosity versus shear rate for mono-dispersed suspensions with particle diameters of 175 μm and 750 μm . It is clearly shown that keeping the same volume fraction， the suspensions with larger particle size has lower viscosity at most of the shear rate. Note. From Making the connection - particle size, size distribution and rheology. [9]

Equations 1.8 and 1.9 are widely referred to as the Krieger-Dougherty equation. As $\phi \xrightarrow{\text{yields}} 0$, Equation 1.8 reduces to Einstein's formula, which is shown in Equation 1.3. If $\phi \xrightarrow{\text{yields}} \phi_m$, then the viscosity $\eta \xrightarrow{\text{yields}} \infty$, which is the close-pack situation. In many papers [14] the maximum volume fraction ϕ_m is called the maximum packing fraction p .

Generally, ϕ_m decreases as η increases, while the product usually remains in the range from 1.4 to 3 [7]. Fletcher and Hill employed a latex/pressure-sensitive adhesive suspension system to study the effects of volume fraction on viscosity, showing that with the increase of volume fraction from 45% to 55% to 61%, the viscosity increases in spite of the shear rate [15].

The above discussions and facts indicate that the viscosity of liquid suspension increases as the volume of the suspended particles in the suspension increases. [16] [17]

1.3 Viscosity And Particle Size Distribution

At a high volume fraction, the viscosity of the liquid suspension has strong dependence on the particle size distribution. To evaluate the effect of the particle size distribution on the effective viscosity, first the contribution of particle size to the effective viscosity of liquid suspension in a monodisperse system needs to be evaluated. In 1950s and 1960s, many theoretical and experimental studies of monodisperse suspensions of particles at micron and sub-micron scales showed that on keeping a constant volume fraction, the viscosity of liquid suspension decreases as the size of the suspended particles increases[18] [19][20].

The phenomenon can be explained by an approach proposed by Dr. Tao and Dr. Xu [16]. At a high ϕ, the particle size distribution has a strong effect on the viscosity. Experiments on monodispersed suspensions of particles on the order of microns and sub-microns show that at constant ϕ, the viscosity goes down as the particle size increases.

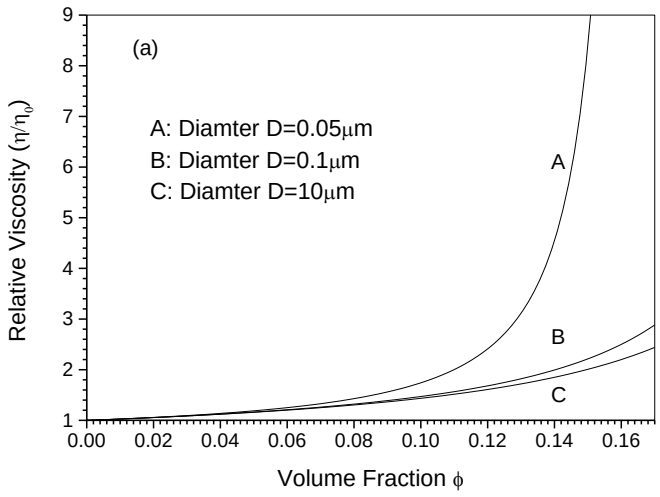

Fig.1.4 The viscosity versus volume fraction and particle size for mono-dispersed suspensions.[16]

As shown in Fig 1.3, for example, at $\phi = 15\%$, a suspension of 10.0 μm particles has a viscosity only 23.9% of the viscosity of a suspension of $0.05\mu m$ particles.

Generally, the effective viscosity depends on how much freedom the suspended particles have in the suspension. The less freedom for the particles, the faster the energy dissipates and the higher the effective viscosity is. The mean separation of the spheres inside the suspension is given by $\frac{a}{\phi^{1/3}}$, where *a* is the particle radius. As *a* gets bigger, the mean separation increases, indicating that the suspended particles have more freedom to move in the suspension. Thus η goes down.

Let us consider a liquid suspension with noninteracting spheres of diameter D suspended in a base liquid of viscosity η_0 go. Since D is on the order of nanometer or micrometer, the particles are classical ones. Because of the thermal vibration, these particles in the base liquid seem to be larger than their actual physical size D. This can be estimated as follows.

From the thermal motion,

$$\frac{1}{2}\mathrm{m}v^2 \approx \frac{3}{2}k_B\mathrm{T} \tag{1.11}$$

We have the average thermal velocity

$$\bar{\mathrm{v}} \approx \sqrt{3\mathrm{k_B}\,\mathrm{T}/\mathrm{m}} \tag{1.12}$$

If the relaxation time is t_0, the length $\lambda = \bar{\mathrm{v}}\mathrm{t}_0$ is the additional dimension due to the thermal motion.

Therefore, in the base liquid, the particles seem to have a diameter,

$$\mathrm{D_x} = \mathrm{D} + \lambda \tag{1.13}$$

Then, the maximum volume fraction to be available for the particles is given by

$$\phi_m = \phi_{m0}(\frac{D}{D_x})^3 \quad (1.14)$$

$$\phi_m = \frac{\phi_{m0}}{(1+\frac{\lambda}{D})^3} \quad (1.15)$$

Where ϕ_{m0} is about 0.64 for random close-packing. It is clear from Eq.(1.15) that as D increases, the maximum volume fraction ϕ_m is increased and the viscosity η is reduced from Eq.(1.10)

1.4 Viscosity And Polydispersity

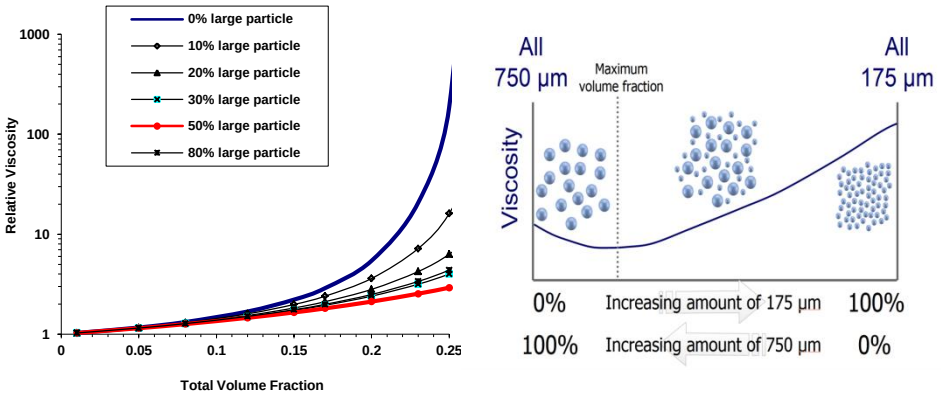

Fig 1.5 For monodisperse particles and for the same volume fraction, the relative viscosity increases as the particle size decreases. For a binary particle size distribution, the minimum viscosity is obtained for a mixture of large and small particles.

The values of ϕ_m in Eq.(1.18) also increases with increasing polydispersity. For example, when the ratio of the large particles to small particles increases in a suspension of binary particle-size distribution, the viscosity reduces significantly (Fig.1.4): At $\phi \geq 50\%$, when this ratio reaches 1:1, the viscosity is reduced more than 50% from the mono-disperse case. A qualitative explanation is as follows: For a binary particle-size distribution, we can consider that the small particles thicken the continuous phase and the next-size-up particles then thicken this phase, and hence

$$\eta = \eta_0(1 - \frac{\phi_1}{\phi_{m1}})^{-[\eta_1]\phi_{m1}}(1 - \frac{\phi_2}{\phi_{m2}})^{-[\eta_2]\phi_{m2}} \qquad (1.16)$$

Which is lower than that of a suspension of uniform small particles with volume fraction $\phi_1 + \phi_2$.

It is clear from the above discussion that aggregating small particles into large ones in a liquid suspension will reduce the effective viscosity while ϕ remains the same. For most suspensions, this aggregation can be realized with either electric or magnetic fields.

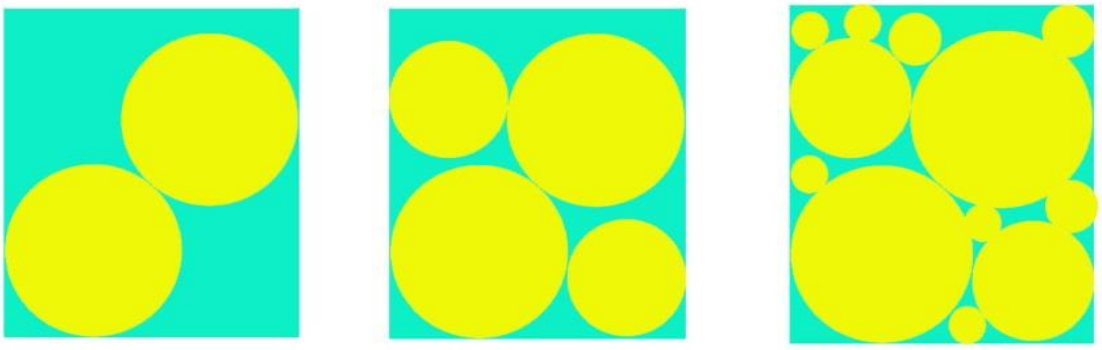

Fig. 1.6 increasing the polydispersity will increase the ϕ_m [30-33]

1.5 Aggregated Short Chains Dramatically Reduce Viscosity

The viscosity of most fluids is isotropic. An important exception is a nematic liquid crystals. When its molecules are aligned by a magnetic field in the field direction, it has very low viscosity along the field direction. In contrast, its viscosity in the directions perpendicular to the magnetic field is very high [27]. The nematic liquid crystal example provides important insight for our case.

Let us consider a liquid suspension which has small spherical particles of radius *a* suspended in a base liquid with viscosity η_0. According to

$$\frac{\eta}{\eta_0} = (1 - \frac{\phi}{\phi_m})^{-[\eta]\phi_m} \tag{1.17}$$

For non-spherical particles, the generalized formula is given by,

$$\frac{\eta}{\eta_0} = (1 - \frac{\phi}{\phi_m})^{-\nu\phi_m} \tag{1.18}$$

where ν is the intrinsic viscosity for the non-spherical particles.

We assume that the suspension is flowing along a pipeline. The viscosity is isotropic not anisotropic, But we can apply an electric filed parallel to the flow direction to aggregate the particles in order to reduce viscosity along the flow direction. According to Dr. Tao and Dr. Xu`s paper, the viscosity of crude oil can be reduced as shown in Fig. 1.1. [16][30-33]

In a small section of the pipeline, we apply a strong electric field parallel to the flow (Fig.1.6).

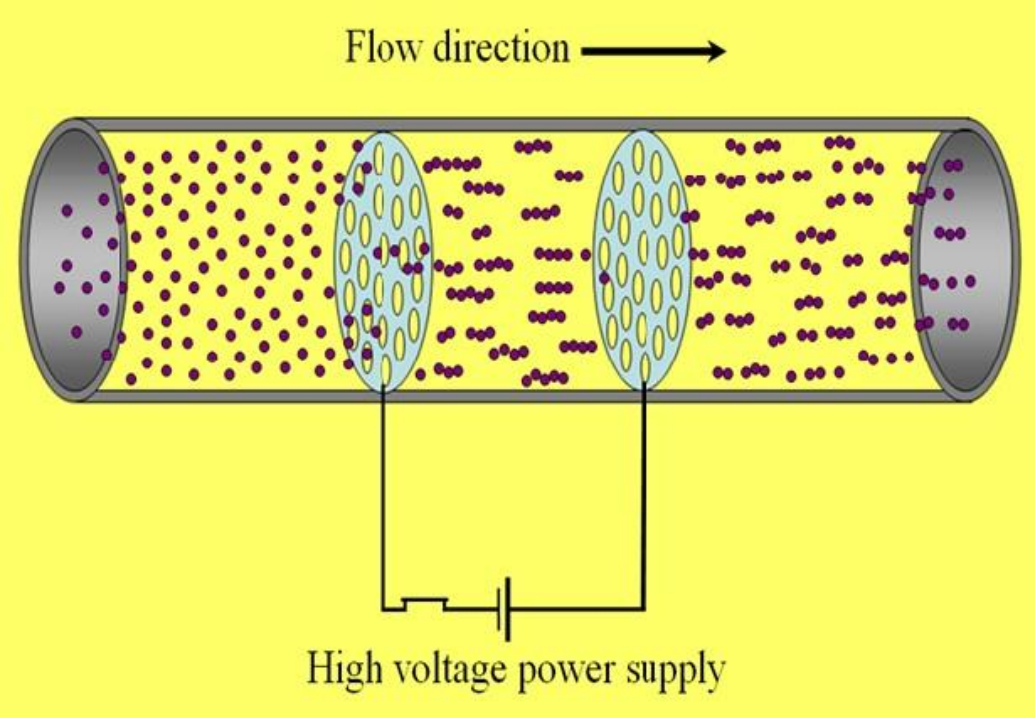

Fig. 1.7 As the liquid suspension flow passes a strong local electric field, the suspended particles are aggregated into short chains along the field direction.

The basic problems are how to aggregate particles and how to confirm that they are aggregated.

1.6 Chained Particles With External Field Reducing The Viscosity Of Liquid Suspension

Since the dielectric constant for the particles ε_p is different from the dielectric constant of the base liquid ε_f, the particles are polarized in the electric field,

$$\vec{p} = \varepsilon_f \overrightarrow{E_{loc}} a^3 \frac{(\varepsilon_p - \varepsilon_f)}{(\varepsilon_p + 2\varepsilon_f)} \tag{1.19}$$

Where $\overrightarrow{E_{loc}}$ is the local electric field acting on the sphere, which is stronger than the applied electric field. In CGS units, the interaction between two induced magnetic dipoles is

$$U = p^2 \frac{(1 - 3cos^2\theta)}{\varepsilon_f r^3} \tag{1.20}$$

where *r* is the distance between the two particle centers and θ is the angle between the field and the line joining the two dipoles. When the two particles align in the field direction and touch each other, $\theta = 0$ and $r = 2a$, U has the minimum,.

$U_{min} = \frac{-p^2}{4\varepsilon_f a^3}$

Before the electric field is applied, the particles are randomly distributed. Therefore, the average distance between two neighbour particles is $n^{-1/3}$, where the particle density $n = \frac{\phi}{\frac{4}{3}\pi a^3}$ If the two particles are not aligned as a chain along the field direction, their dipolar interaction energy is U_i, $U_i > U_{min}$. The probability for two neighbouring particles to aggregate is estimated as

$$\frac{1}{1 + \frac{\exp(U_{min} - U_i)}{k_B T}} \tag{1.21}$$

As $U_{min} - U_i$ is negative and increases with the applied electric field, a strong electric field will force the particles to aggregate into short chains along the field direction.

In ER fluids, after a strong electric field is applied, the suspended particles quickly form chains and the chains aggregate into thick columns. The whole process only takes a couple of milliseconds [28][29]. While the field induced dipolar interaction in other liquid suspensions is not as strong as that in ER fluids, the basic physics remains the same. For example, in asphalt base crude oil, the asphalt particles have $\varepsilon_p = 2.7$ while the base liquid, gasoline, has $\varepsilon_f = 2.0$. If the asphalt particle absorbs moisture, their dielectric constant is further increased. In paraffin base crude oil, the base liquid gasoline has $\varepsilon_f = 2.0$, the paraffin wax particles have dielectric constant 2.5, and the suspended sulphur dioxide particles have dielectric constant 15. Therefore, in a strong electric field, these particles are polarized and aggregate into short chains.

Now let us estimate the required time for such aggregation. The force between two neighboring particles is about $\frac{6p^2 n^{\frac{4}{3}}}{\varepsilon_f}$. From this force and the Stoke's drag force $6a\pi\nu\eta_0$ we estimate the particle's average velocity $\nu = \frac{p^2 n^{\frac{4}{3}}}{a\pi\eta_0\varepsilon_f}$. The time required for two neighboring particles to come together is about

$$\tau = \frac{n^{-\frac{1}{3}}}{\nu} = \frac{\pi(\frac{4}{3}\pi\phi)^{\frac{5}{3}}\eta_0(\varepsilon_p+2\varepsilon_f)^2}{\varepsilon_f(\varepsilon_p-\varepsilon_f)^2 {E_{loc}}^2} \qquad (1.22)$$

Take asphalt base crude oil as an example. With $\varepsilon_p = 2.7$, $\varepsilon_p = 2.0$, $\phi = 0.5$, $\eta_0 =$ 1poise, and $E_{loc} = 1000V/mm$, we have τ around 4.5 seconds. When the particles stay inside the electric field for a time longer than τ, the particles will be aggregated into short chains. Therefore, the aggregation for crude oil is quite fast. [30-33]

References:

[1] Landau, L.D. & Lifshitz, E.M. (1959). In, Fluid mechanics. New York: Pergamon Press.

[2] http://www.merriam-webster.com/dictionary/viscosity

[3] Symon, Keith (1971). Mechanics (Third ed.). Addison-Wesley. ISBN 0-201-07392-7.

[4] https://en.wikipedia.org/wiki/Viscosity

[5] http://www.engineeringtoolbox.com/dynamic-absolute-kinematic-viscosity-d_412.html

[6] Einstein, A. (1905). A New Determination of Molecular Dimensions. Annalen der Physik, 17(4), 549-560.

[7] Larson, R. G. (1999). Particulate Suspensions. In, K. E. Gubbins et al. (Eds.), The Structure and Rheology of Complex Fluids (pp. 263-323). New York: Oxford University Press.

[8] Hiemenz, P. C. (1986). The Viscosity of Dilute Dispersions. In J. J. Lagowski (Ed.), Principles of Colloid and Surface Chemistry (2nd ed.). (pp. 169-222). New York: Marcel Dekker.

[9] Huang, Ke Colin (2010) Electrorheology for Energy Production and Conservation

[10] Hunter, R. J. (1993). Flow Behaviour. In, Introduction to Modern Colloid Science (pp.97-130). New York: Oxford University Press. 150

[11] Mooney, M. (1951). The Viscosity of A Concentrated Suspension of Spherical Particles. Jounal of Colloid Science, 6(2), 162-170.

[12] Krieger, I. M., & Dougherty, T. J. (1959). A Mechanism for Non-Newtonian Flow in Suspensions of Rigid Spheres. Transaction of the Society of Rheology, 3(1), 137-152.

[13]https://en.wikipedia.org/wiki/Random_close_pack

[14] Fitch, R. M. (1997). Rheology of Polymer Colloids. In R. H. Ottewill & R. L. Rowell (Eds.), Polymer Colloids (pp. 277-313). San Diego, CA: Academic Press. 149

[15] Fletcher, J., & Hill, A. (n.d.). Making the connection - particle size, size distribution and rheology. Retrieved February 25, 2009, from ttp://www.chemeurope.com/articles/e/61207/?WT.mc_id=ca0102

[16]R. Tao and X. Xu, Energy & Fuels, 20, 2046-2051 (2006).

[17] R. Tao, International J. of Modern Physics B, V. 21, N28&29, pp4767-4773 (2007).

[18] Saunders, F. L. (1961). Rheological Properties of MonodisperseLatex Systems I. Concentration Dependence of Relative Viscosity. Jounal of Colloid Science, 16(1), 13-22.

[19] Sweeny, K. H., & Geckler, R. D. (1954). The Rheology of Suspensions. Jounal of Applied Physics, 25(9), 1135-1144.

[20] Thomas, D. G. (1965). Transport characteristics of suspension: VIII. A note on the viscosity of Newtonian suspensions of uniform spherical particles. Jounal of Colloid Science, 20(3), 267-277.

[21] B. Hof, J. Westerweel, T. W. Schneider, and B. K. Eckhardt, Finite lifetime of turbulence in shear flows, Nature 443, 59 (2006).

[22] K. Avila, D. Moxey, A. de Lozar, M. Avila, D. Barkley, The Onset of Turbulence in Pipe Flow, Science 333, 192 (2011).

[23] B. Hof , A. de Lozar, M. Avila, X. Y. Tu, T. M. Schneider, Eliminating Turbulence in Spatially Intermittent Flows, Science 327, 1491 (2010).

[24] D. Vergano,, Turbulence theory gets a bit choppy, USA Today. September 10 (2006).

[25] https://en.wikipedia.org/wiki/Pipeline_transport

[26] https://www.cia.gov/library/publications/the-world-factbook/fields/2117.html

[27] M. Miesowicz, The Three Coefficients of Viscosity of Anisotropic Liquids, Nature 158, 27 (1946).

[28]R. Tao and J. M. Sun, Three-dimensional Structure of Induced Electrorheological Solid, Phys. Rev. Lett. 67, 398 (1991).

[29]T. J. Chen, R. N. Zitter, and R. Tao, Laser Diffraction Determination of the Crystalline Structure of an Electrorheological Fluid, Phys. Rev. Lett. 68, 2555 (1992).

[30] Du, E., Tang, H., Huang, K. and Tao, R., Reducing the viscosity of diesel fuel with electrorehological effect, Journal of Intelligent Material Systems and Structures.53, 59 (2011)

[31] Huang, K., Du, E., Tang, H. and Tao, R., Electrorheology improves E85-engine performance and efficiency, Journal of Intelligent Material Systems and Structures. 60,67 (2011)

[32] R. Tao and G. Q. Gu, Suppressing turbulence and enhancing liquid suspension flow in pipelines with electrorheology, Phys. Rev. E 91, 012304 (2015)

[33] Tao, R.; Du, E.; Tang, H.; Xu, X., Neutron scattering studies of crude oil viscosity reduction with electric field, Fuel, 134, 493,498 (2014)

CHAPTER 2

NEUTRON SCATTERING THEORY AND SANS TECHNIQUE

Both neutrons and protons are nucleons, which are attracted and bound together by the nuclear force to form atomic nuclei. The neutron has a mass of about 1.675×10^{-27} kg, has a mean radius of about 0.8×10^{-15} m, has spin $\frac{1}{2}$ and a magnetic moment of -1.9132 nuclear magnetons. [1] [2] [3] The neutron has no net electric charge. The proton has a positive electric charge and is directly influenced by electric fields, while the response of the neutron to this force is much weaker. A free neutron is unstable with a mean lifetime of just under 15 minutes and decays into a proton, an electron and an antineutrino. Since the neutron has no net electric charge and only has a magnetic moment, its interactions with matter are confined to the short-range nuclear and magnetic interactions. Since its interaction cross section is small, the neutron usually penetrates well through matter, making it a unique probe for investigating bulk condensed matter.

Neutrons are a bulk probe for investigating both structures and dynamics. Some of the advantages of neutrons as a probe for condensed matter follow. First, neutrons interact through short-range nuclear interactions. They are very penetrating and do not heat up samples; Neutrons are good probes for investigating structures in condensed matter; Second, neutron wavelengths are comparable to atomic sizes, neutron can be a atomic scale tool; Third, neutrons are good probes to investigate the dynamics of solid state and liquid materials; Finally, neutron interactions with hydrogen and deuterium are widely different, making the deuterium labeling method an advantage. With these properties, the neutron is the best tool for us to investigate crude oil structure changing.

2.1 The Schrödinger Equation With Born Approximation

We can understand neutron scattering theory by solving the Schrödinger equation with the Born Approximation. So let's start with the solution of the Schrödinger equation with perturbation theory.

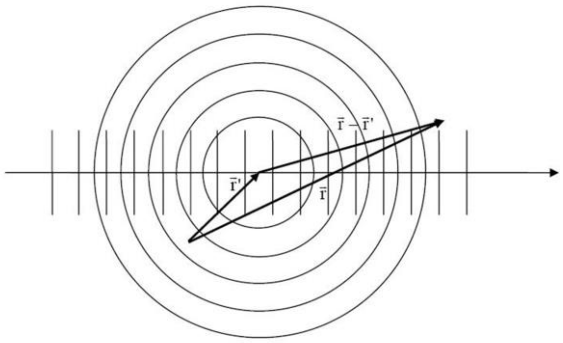

Fig. 2.1: Incident wave (plane wave) and scattered wave (spherical wave).

The Schrödinger equation is expressed as follows:

$$\begin{aligned} H_i\psi_i &= E_i\psi_i \\ H\psi &= E_S\psi \\ H &= H_i + V \end{aligned} \qquad (2.1)$$

H is the full Hamiltonian operator, H_i is the incident neutron kinetic energy operator and V is the neutron-nucleus interaction potential. E_i and E_S are the eigenvalue energies for the incident neutron and for the scattered neutron. ψ_i and ψ are the eigenfunctions for the incident (non-interacting) neutron and for the interacting neutron-nucleus pair.

$$\begin{aligned} H_i &= \frac{p^2}{2m} = -\frac{\hbar^2}{2m}\nabla^2 \\ E_i &= \frac{\hbar^2 k_i^2}{2m} \end{aligned} \qquad (2.2)$$

where $\vec{p} = -i\hbar\vec{\nabla}$ is the momentum operator for the neutron.
From equation (2.1) and (2.2)

$$(H_i - E_i)\Psi_i(\vec{r}) = -\frac{\hbar^2}{2m}(\nabla^2 + k_i^2)\Psi_i(\vec{r}) = 0 \qquad (2.3)$$

The solution is an incident plane wave $\Psi_i(\vec{r}) = \exp(i\vec{k_i}\cdot\vec{r})$ using vector notation. The full differential equation is written as:

$$(\nabla^2 + k_s^2)\Psi(\vec{r}) = \frac{2m}{\hbar^2}V(\vec{r})\Psi(\vec{r}) \tag{2.4}$$

Its solution is an integral equation of the form:

$$\Psi(\vec{r}) = \Psi_i(\vec{r}) + \left(\frac{2m}{\hbar^2}\right)\int d\vec{r}' G(\vec{r} - \vec{r}')V(\vec{r}')\Psi(\vec{r}') \tag{2.5}$$

where $G(\vec{r} - \vec{r}')$ is a Green's function satisfying the following differential equation:

$$(\nabla^2 + k_s^2)G(\vec{r}) = \delta(\vec{r}) \tag{2.6}$$

k_s ks is the scattered neutron wave number. Its solution is a spherical outgoing wave of the form:

$$G(\vec{r}) = -\frac{1}{4\pi}\frac{\exp(ik_s r)}{r} \tag{2.7}$$

In order to verify this result, the following relations valid in spherical coordinates are used:

$$\nabla\left(\frac{1}{r}\right) = -\frac{\hat{r}}{r^2}$$

$$\nabla^2\left(\frac{1}{r}\right) = \frac{1}{r^2}\left[\frac{\partial}{\partial r}r^2\left(\frac{\partial}{\partial r}\right)\right]\left(\frac{1}{r}\right) = -4\pi\delta(\vec{r}) \tag{2.8}$$

Therefore, we obtain:

$$\Psi(\vec{r}) = \Psi_i(\vec{r}) - \left(\frac{m}{2\pi\hbar^2}\right)\int d\vec{r}' \frac{\exp(ik_s|\vec{r} - \vec{r}'|)}{|\vec{r} - \vec{r}'|}V(\vec{r}')\Psi(\vec{r}') \tag{2.9}$$

Vector $\vec{r}'$ is within the sample and $\vec{r}$ is far from the sample so that $r >> \vec{r}'$ and therefore one can approximate

$$|\vec{r} - \vec{r}'| \cong r - \frac{\vec{r}\cdot\vec{r}'}{r}$$

$$\frac{\exp(ik_s|\vec{r} - \vec{r}'|)}{|\vec{r} - \vec{r}'|} = \frac{\exp(ik_s r)}{r}\exp\left(-\frac{ik_s\vec{r}\cdot\vec{r}'}{r}\right) = \frac{\exp(ik_s r)}{r}\exp\left(-i\vec{k}_s\cdot\vec{r}'\right) \tag{2.10}$$

Here, the scattered neutron wave vector k_s has been defined as $\vec{k}_s = \frac{k_s\vec{r}}{r}$.

The general solution of the Schrödinger equation is an integral equation that can be solved iteratively through the expansion:

$$\Psi(\vec{r}) = \Psi_i(\vec{r}) - \left(\frac{m}{2\pi\hbar^2}\right)\int d\vec{r}' G(\vec{r} - \vec{r}')V(\vec{r}')\Psi_i(\vec{r}') + \left(\frac{m}{2\pi\hbar^2}\right)^2\int d\vec{r}' G(\vec{r} - \vec{r}')V(\vec{r}')\int d\vec{r}'' G(\vec{r} - \vec{r}'')\Psi_i(\vec{r}'') + \ldots \tag{2.11}$$

Keeping only the first integral term corresponds to the first Born approximation which can be presented in the form:

$$\Psi(\vec{r}) = \Psi_i(\vec{r}) - \left(\frac{m}{2\pi\hbar^2}\right)\int d\vec{r}' G(\vec{r}-\vec{r}')V(\vec{r}')\Psi_i(\vec{r}')$$

$$\Psi(\vec{r}) = \exp(i\vec{k_i}\cdot\vec{r}) + \frac{\exp(ik_s r)}{r}\left(\frac{m}{2\pi\hbar^2}\right)\int d\vec{r}' \exp\left(-i\vec{k_s}\cdot\vec{r}'\right)V(\vec{r}')\exp(i\vec{k_i}\cdot\vec{r})$$

$$\Psi(\vec{r}) = \exp(i\vec{k_i}\cdot\vec{r}) + \frac{\exp(ik_s r)}{r} f(\theta) \qquad (2.12)$$

The scattering amplitude f(θ) has been defined as:

$$f(\theta) = \left(\frac{m}{2\pi\hbar^2}\right)\int d\vec{r}' \exp\left(-i\vec{Q}\cdot\vec{r}'\right)V(\vec{r}') \qquad (2.13)$$

$\vec{Q} = \vec{k}_s - \vec{k}_i$ is the scattering vector. $f(\theta)$ is the Fourier transform of the interaction potential $V(\vec{r}')$. $f(\theta)$ has been assumed to be independent of the azimuthal angle φ.

The first Born approximation applies to thermal/cold neutrons neutron scattering corresponding to "s wave" scattering (i.e., corresponding to a zero orbital angular quantum number). This includes all of neutron scattering except for neutron reflectivity where higher order terms in the Born expansion have to be included. Neutron reflectometry involves refraction (not diffraction). $\vec{Q}$ characterizes the probe length scale and its magnitude is given for elastic scattering in terms of the neutron wavelength λ and scattering angle θ as $Q = (4\pi/\lambda)\sin(\theta/2)$. For small angles (SANS), it is simply approximated by $Q = 2\pi\theta/\lambda$. Since Q is the Fourier variable (in reciprocal space) conjugate to scatterer positions (in direct space), investigating low-Q probes large length scales in direct space and vice versa. In summary, the solution of the Schrodinger equation is an incident plane wave plus a scattered spherical wave multiplied by the scattering amplitude.

2.2 Scattering Cross Sections

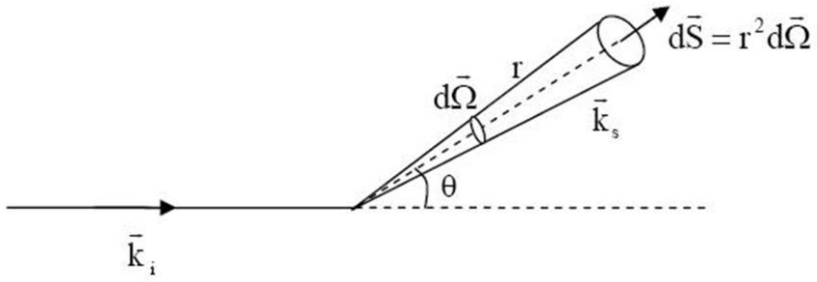

Fig. 2.2: Representation of neutrons scattered with angle θ inside a solid angle dΩ.

Consider incident neutrons of wavenumber k_i and scattered neutrons of wavenumber k_s. The incident neutron flux also called current density (neutrons/cm^2.s) is given by:

$$\vec{J}_i = \frac{i\hbar}{2m}(\Psi_i \vec{\nabla}\Psi_i^* - \Psi_i^* \vec{\nabla}\Psi_i) \tag{2.14}$$

$$\Psi_i(\vec{r}) = \exp(i\vec{k}_i \cdot \vec{r}) \tag{2.15}$$

is the incident plane wave. Performing the simple operation $\vec{\nabla}\Psi_i(\vec{r}) = i\vec{k}_i\Psi_i(\vec{r})$, one obtains

$$\vec{J}_i = \hbar\vec{k}_i / m \tag{2.16}$$

Similarly for the scattered neutron flux:

$$\vec{J}_s = \frac{i\hbar}{2m}(\Phi\vec{\nabla}\Phi^* - \Phi^*\vec{\nabla}\Phi) \tag{2.17}$$

Where $\Phi = \Psi - \Psi_i = \frac{\exp(ik_s r)}{r} f(\theta)$. Here also, performing the differentiations, one obtains:

densities J_i

$$\vec{J}_i = \frac{\hbar\vec{k}_s}{m}\frac{|f(\theta)|^2}{r^2} \tag{2.18}$$

The differential neutron scattering cross section is defined as:

$$d\sigma_s(\theta) = \frac{J_s r^2 d\Omega}{J_i}\vec{J}_i = \frac{k_s}{k_i}|f(\theta)|^2 d\Omega \tag{2.19}$$

This is the ratio of the neutron flux scattered in dΩ over the incident neutron flux. Within the first Born approximation (also called the Fermi Golden Rule):

$$\frac{d\sigma_s(\theta)}{d\Omega} = \frac{J_s r^2 d\Omega}{J_i}\vec{J}_i = \frac{k_s}{k_i}|f(\theta)|^2 \tag{2.20}$$

$$\frac{d\sigma_s(\theta)}{d\Omega} = \frac{J_s r^2 d\Omega}{J_i}\vec{J}_i = \frac{k_s}{k_i}\left|\left(\frac{m}{2\pi\hbar^2}\right)\int d\vec{r}' \exp\left(-i\vec{Q}\cdot\vec{r}'\right)V(\vec{r}')\right|^2$$

This cross section contains information about what inhomogeneities are scattering and how they are distributed in the sample. The microscopic total scattering cross section is its integral over solid angles:

$$\sigma_s = \int\left(\frac{d\sigma_s(\theta)}{d\Omega}\right)d\Omega \tag{2.21}$$

Cross sections are given in barn units (1 barn = 10^{-24} cm^2).

Given the (atomic) number density N/V (number of scattering nuclei/cm^3) in a material, a macroscopic cross section is also defined as: $\sum_s = (N/V)\sigma_s$ (units of cm^{-1}). SANS data are often presented on an "absolute" macroscopic cross section scale independent of instrumental conditions and of sample volume. It is given by $d\sum_s/d\Omega = (N/V)\, d\sigma_s/d\Omega$

2.3. Simple Model For Neutron Scattering Lengths

A simple argument is used here in order to appreciate the origin of the scattering length (Squires, 1978). Consider a neutron of thermal/cold incident energy E_i being elastically scattered from a nucleus with an attractive square well potential $-V_0$ (note that $V_0 >> E_i$). Recall the Schrödinger equation for this simplest potential.

$$\left[-\frac{\hbar^2}{2m}\nabla^2 + V(r)\right]\Psi(\vec{r}) = E_s\Psi(r) \tag{2.22}$$

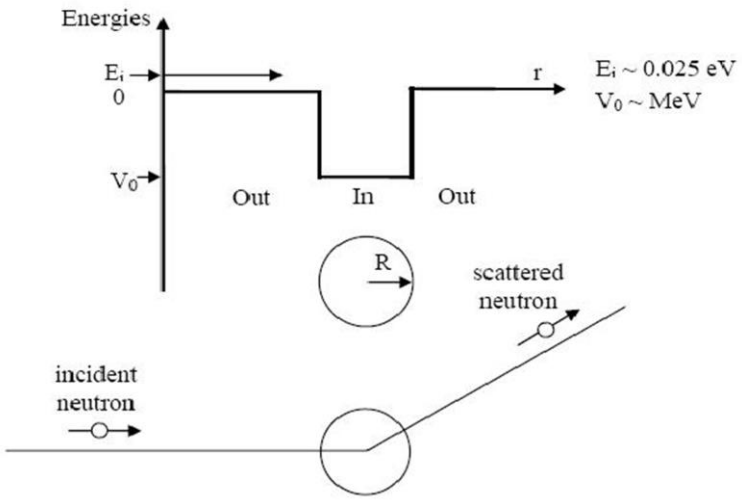

Fig. 2.3: Neutron scattering from the quantum well of a nucleus.

Small-Angle Neutron Scattering (SANS) is a technique of choice for the characterization of structures in the nanoscale size range. This covers structures from the near Angstrom sizes to the near micrometer sizes. They are typically from 0.2 degree to 20 degree and cover two orders of magnitude in two steps. A low-Q configuration covers the first order of magnitude (0.2^o to 2^o) and a high-Q configuration covers the second one (2^o to 20^o). The scattering variable is defined as $Q = (4\pi/\lambda)\sin(\theta/2)$ where λ is the neutron wavelength and θ is the scattering angle. Within the small-angle approximation, Q simplifies to $Q = 2\pi\theta/\lambda$. The SANS scattering variable Q range is typically from $Q = 2\pi\theta/\lambda$ 0.001 $Å^{-1}$ to 0.45 $Å^{-1}$. This corresponds to d-spacings from 6,300 Å down to 14 Å. Scattering measurements are performed in the Fourier (also called reciprocal) space, not real space like microscopy. For this, scattering data have to be either inverted back to real space or fitted to models describing structures in reciprocal space. Scattering methods measure correlation functions. These are not the Fourier transform of the density of inhomogeneities within the sample. They are the density-density correlation functions instead. It should be noted that because of this, the "phase" information is completely lost. It is not possible to reconstruct a complete image of the sample structure by scattering from one sample. Trying to recover phase information is complicated and involves measuring a series of samples with identical structures but different contrasts.

2.4 Measurements Of Neutron Scattering Lengths

Note that the index of refraction n is related to the material atomic density ρ (atoms/cm^3), the neutron scattering length b, and the neutron wavelength λ as:

$$n = 1 - \frac{\rho b}{2\pi}\lambda^2 \qquad (2.23)$$

The scattering length b can be measured by measuring the index of refraction n using optical methods. Note that most materials have an index of refraction less than one for neutrons and greater than one for light. Neutron interferometry methods are another way of measuring scattering lengths.

2.5 Comparing SANS To Other Techniques

The advantage of SANS over other small-angle scattering methods (such as small-angle xray or light scattering) is the deuteration method. This consists in using deuterium labeled components in the sample in order to enhance their contrast. This is reminiscent of contrast variation in microscopy whereby the level of light incident upon a sample is varied using a diaphragm. SANS can measure either naturally occurring contrasts or artificial contrasts introduced through deuteration. Labeling is difficult to achieve with x-rays (SAXS) since this involves heavy atom labels that change the sample drastically. SANS can measure density fluctuations and composition (or concentration) fluctuations. SAXS can measure only density fluctuation. The deuteration method allows this bonus.

SANS is disadvantaged over SAXS by the intrinsically low flux of neutron sources (nuclear reactors or spallation sources using cold source moderators) compared to the orders of magnitude higher fluxes for x-ray sources (rotating anode or synchrotrons). Neutron scattering in general is sensitive to fluctuations in the density of nuclei in the sample. X-ray scattering is sensitive to inhomogeneities in electron densities whereas light scattering is sensitive to fluctuations in polarizability (refraction index). Microscopy has the advantage that data are acquired in direct (real) space whereas scattering methods (such as SANS) measure in reciprocal space. Electron microscopy (EM) and SANS are complementary methods. EM is applied on very thin samples only, it cannot measure samples at different concentrations and temperatures directly, and the observed images are a 2D projection. SANS can do all these things but cannot produce an image in real space. SANS data analysis is performed at many levels. The initial level consists of

"follow the trends" type of approach using standard plot methods. The next level uses nonlinear least squares fits to realistic models. The final trend makes use of sophisticated ab-initio or "shape reconstruction" methods in order to obtain insight into the structure and morphology within the investigated sample. Oftentimes, it takes independent information obtained from other methods of characterization to obtain a thorough understanding of SANS data because "most SANS data look alike". SANS is not known for abundance in scattering peaks (unlike singlecrystal diffraction, Nuclear Magnetic Resonance, Infra-Red spectroscopy, etc) but enough features (i.e., "clues") are available. Available models describe scattering from compact shape objects in dilute or concentrated systems as well as "non-particulate" scattering such as in the case of gel-like or porous media. SANS has been used for single-phase as well as multi-phase systems. Phase transitions have been investigated as well as the thermodynamics of demixing.

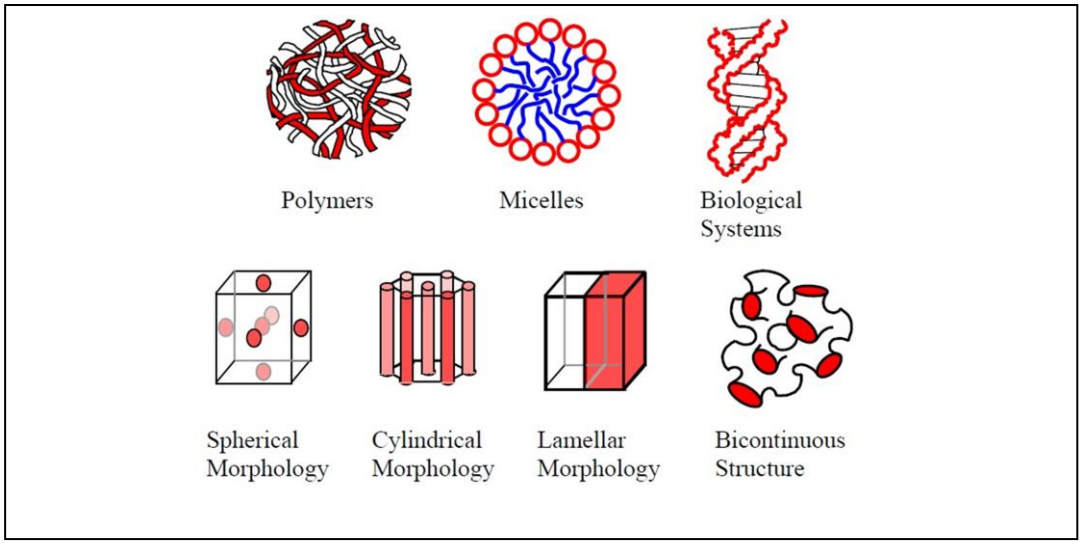

Fig. 2.4 : Various classes of samples and morphologies investigated by SANS.

SANS involves the basic four steps used in all scattering techniques: monochromation, collimation, scattering and detection. Monochromation is performed mostly using a velocity selector. Collimation is preformed through the use of two apertures (a source aperture and a sample aperture) placed far (meters) apart. Scattering is performed from either liquid or solid samples. Detection is performed using a neutron area detector inside an evacuated scattering vessel. The large collimation and scattering distances make SANS instruments are very large (typically 30 m long) compared to other scattering instruments.

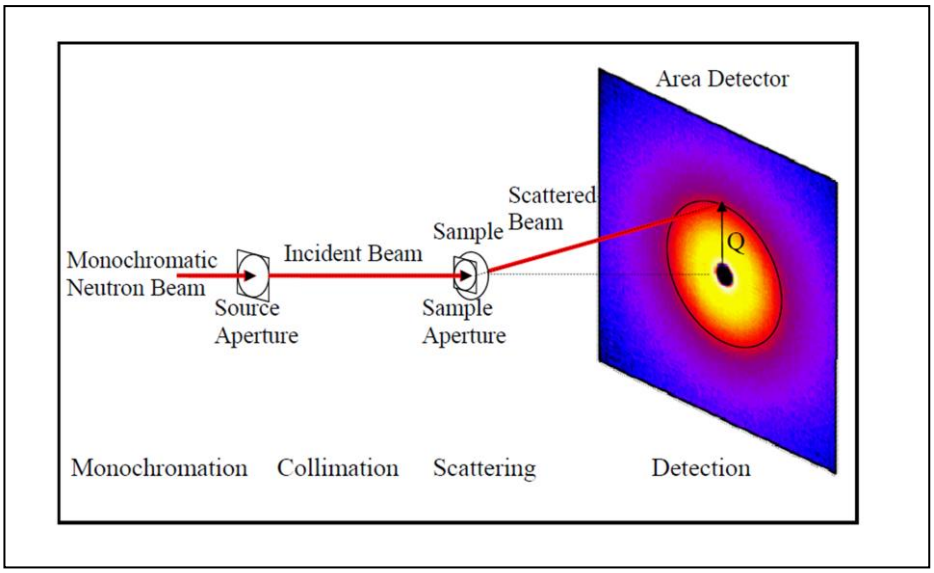

Fig. 2.5 This figure represents the schematics of the SANS technique.

Thus, the vertical sizes are in centimeters whereas horizontal distances are in meters. The SANS technique has been an effective characterization method in many area of research including Polymers, Complex Fluids, Biology, and Materials Science. Other areas such as magnetism also benefited from SANS. SANS instruments have been essential components for any neutron scattering facility for almost three decades. They provide the main justification for the growth and prosperity and are highly oversubscribed. New sample environments have given new momentum to the technique. These include in-situ shear cells, flow cells and rheometers, pressure cells, electromagnets and superconducting magnets, vapor pressure cells, humidity cells, in-situ

reaction cells, etc. New advances in electronics, data handling methods and computers have made SANS a sophisticated “user friendly” characterization method for the non-experts and for “routine” characterization as well as cutting edge research.

2.6 The Measured Macroscopic Scattering Cross Section

Consider a simple scattering system consisting of globular (think spherical) inhomogeneities in a matrix (think solvent). If this system is assumed to be incompressible, the SANS coherent macroscopic scattering cross section (scattering intensity in an absolute scale) can be modeled as:

$$\frac{d\sum_C(Q)}{d\Omega} = \left(\frac{N}{V}\right) V_p^2 \Delta\rho^2 P(Q) S_I(Q) \qquad (2.27)$$

(N/V) is the number density of particles, V_p is the particle volume, $\Delta\rho^2$ is the contrast factor, $P(Q)$ is the single particle form factor and $S_I(Q)$ is the inter-particle structure factor. Note that $P(Q)$ and $S_I(Q)$ are normalized as follows: $P(Q \to 0) = 1$, $P(Q \to \infty) = 0$ and $S_I(Q \to \infty) = 1$. $S_I(Q)$ has a peak corresponding to the average particle inter-distance (the so-called coordination shell) in the case of "concentrated" system where the particle inter-distance is of the same order as the particle size. The inter-distance is much larger than the particle size for "dilute" system.

The incoherent scattering cross section $d\sum_i / d\Omega = \sum_i / 4\pi$ is a constant (Q-independent) background to be added to the coherent scattering level. Its contribution is mostly from hydrogen scattering in the sample.

2.7 Neutron Contrast Conditions

Consider a scattering system made of spheres in a solvent background. The following figures consider four types of contrast conditions:

(1) finite contrast:

(2) zero contrast for two component systems:

(3) multiple contrasts and:

(4) the scattering length density match condition for three component systems. The scattering length density match condition corresponds to zero contrast for the blue spheres.

References

[1]Mohr, P.J.; Taylor, B.N. and Newell, D.B. (2011), "The 2010 CODATA Recommended Values of the Fundamental Physical Constants" (Web Version 6.0). The database was developed by J. Baker, M. Douma, and S. Kotochigova. (2011-06-02). National Institute of Standards and Technology, Gaithersburg, Maryland 20899

[2]Povh, B.; Rith, K.; Scholz, C.; Zetsche, F. (2002). *Particles and Nuclei: An Introduction to the Physical Concepts*. Berlin: Springer-Verlag. p. 73. ISBN 978-3-540-43823-6.

[3] Paul Allen Tipler, Ralph A. Llewellyn (2002). *Modern Physics* (4 ed.). Macmillan. p. 310. ISBN 0-7167-4345-0.

[4]30m SANS: "The 30 m Small-Angle Neutron Scattering Instruments at the National Institute of Standards and Technology", Glinka CJ, et al. *J Appl. Cryst.* 31(3), 430 (1998).

[5]USANS: "Design and performance of a thermal-neutron double-crystal diffractometer for USANS at NIST", Barker JG, et al. *J Appl. Cryst.* 38(6), 1004 (2005).
"Reduction and Analysis of SANS and USANS Data using Igor Pro", Kline, S. R. *J Appl. Cryst.* 39(6), 895 (2006).

[6]B. Hammouda, “SANS from Polymers Tutorial”, NIST Center for Neutron Research Report (1995)

[7] "Reduction and Analysis of SANS and USANS Data using Igor Pro", Kline, S. R. J Appl. Cryst. 39(6), 895 (2006).

[8] We acknowledge the support of the National Institute of Standards and Technology, U.S. Department of Commerce, in providing facilities used in this work.

CHAPTER 3

NIST SANS INSTRUMENTATION

The first SANS instruments were developed over 35 years ago. Small angle neutron scattering instruments should really be called low-Q instruments. The scattering variable Q can be expressed:

$$Q = {}^{2\pi\theta}/_{\lambda} \tag{3.1}$$

λ: neutron wavelength

θ: scattering angle

With either through the use of small angles or long wavelengths or both of them, we can get low Q. Long wavelengths, that is, slow neutron, we can realize it by select slow neutrons from source and cold down the source. At the same time, we need good collimation and good resolution area detectors in order to obtain small angles. Good collimation can be achieved through the use of long neutron flight paths before and after the sample. That is a reason why SANS is up to 30m long.

Fig. 3.1 neutron guide, chamber and detector of facility of NG7 at NIST for Small Angle Neutron Scattering

NG7 is a split-core geometry nuclear fission reactor, that is, thermal neutron beam tubes do not look at the fuel elements directly. This helps minimize epithermal neutrons and gamma radiation in the beams. But this is not enough to get "Cold" neutrons. "Cold" (slow) neutrons are often needed for better spatial resolution in scattering applications. A good moderator is liquid hydrogen. Cold is necessary for slow neutrons. Through inelastic scattering with liquid hydrogen, the Maxwellian neutron spectral distribution is shifted to lower energies, with peaking at 1.8 Å for thermal neutrons.

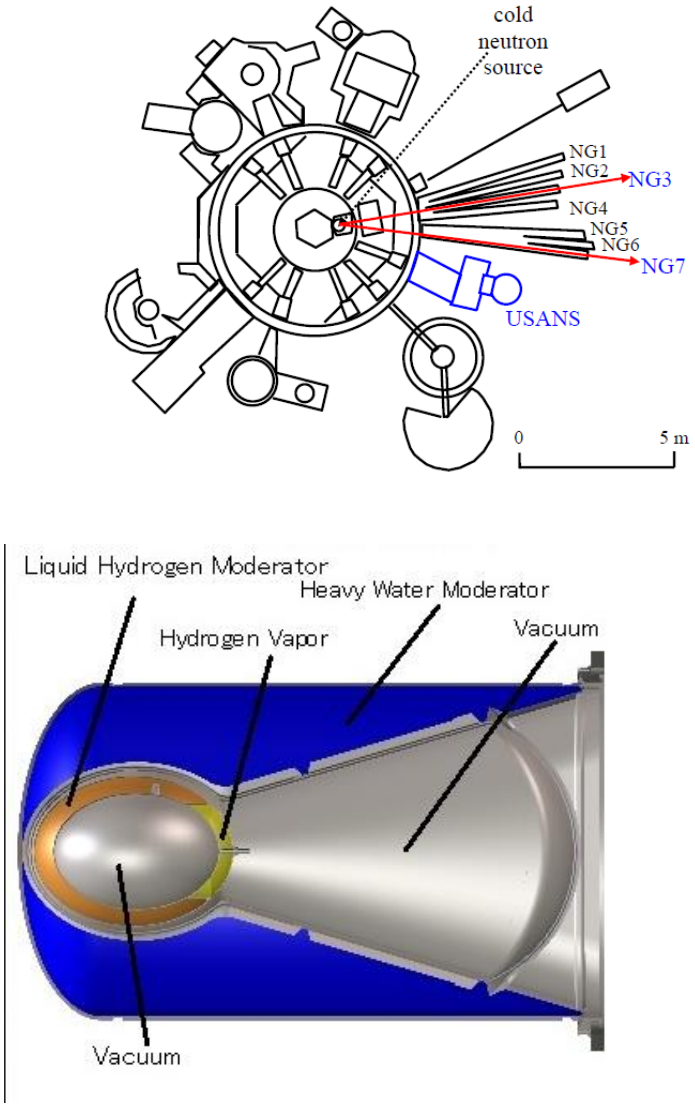

Fig. 3.2 split-core geometry nuclear fission reactor and liquid hydrogen cold source[1][2]

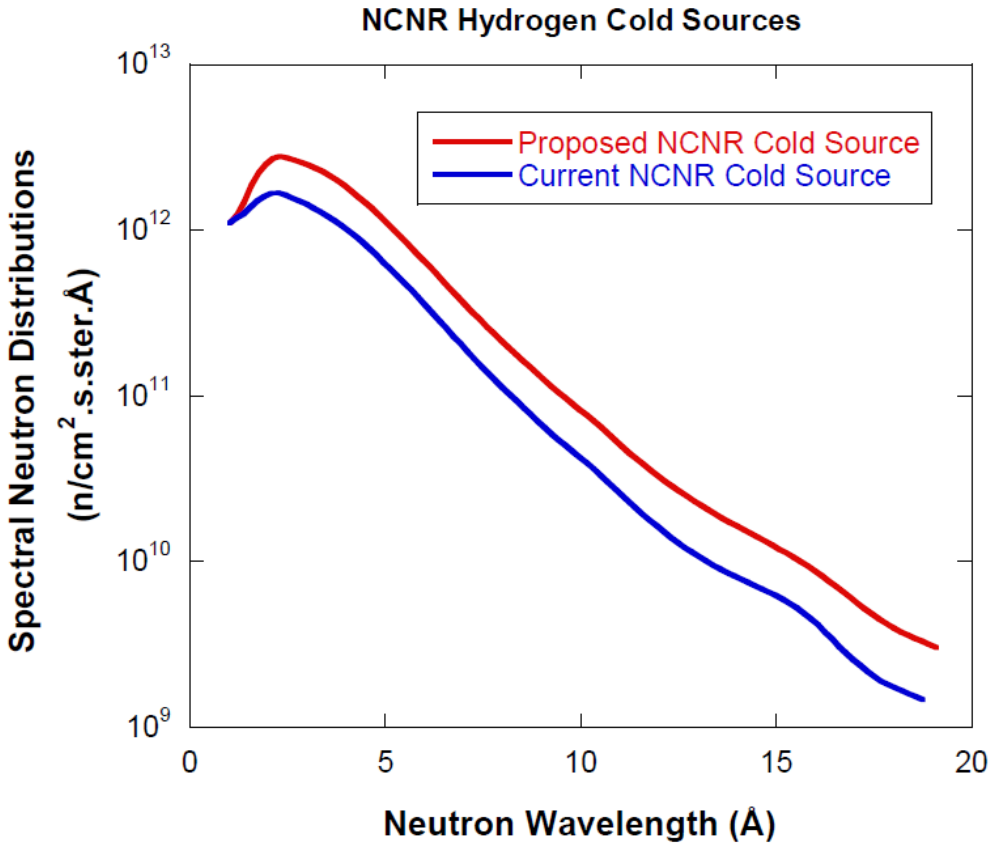

Fig. 3.3 NCNR hydrogen neutron source

3.1. SANS Instrument Components Neutron Guides

Neutrons from the cold source were transported to the entrance of scattering instruments with little loss through Ni or Ni- 58 coated neutron guides, which have a wider critical angle for reflection.

Beam filters

Unwanted epithermal neutrons and gamma rays were cleaned up by high-Z materials, which can stop gammas, and Be, which can transmit neutrons with wavelengths > 4 Å. At the same time, if a curved guide is used, no crystal filter is needed because there is no direct line-of-sight from the reactor source (no gammas in the beam). Curved guides transmit only wavelengths above a cutoff value (no epithermal neutrons in the beam). Typical crystal filter thickness is between 15 cm and 20 cm. For better efficiency, filters are cooled down to liquid nitrogen temperature (77 K = -196 ^{o}C).

Optical filters

Optical filters steer a neutron beam away from the direct line-of-sight and replace crystal filters. They consist of tapered neutron guides that transmit only neutrons that are reflected. They have the advantage of gains in flux over crystal filters at long wavelengths.

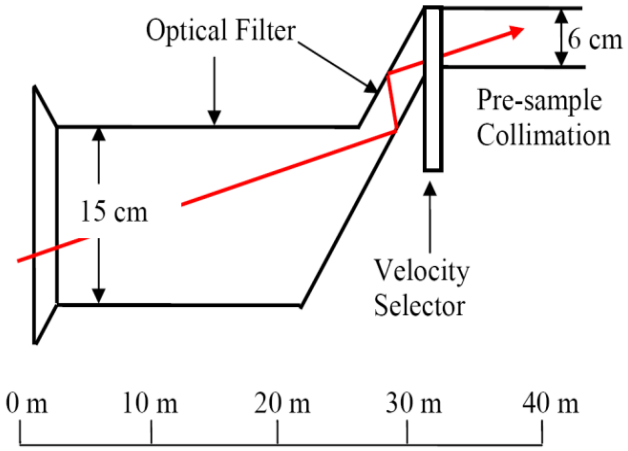

Fig. 3.4 This figure represents the schematics of the SANS technique.

3.2. Velocity Selector

The basic concept for velocity selectors is to allow neutrons to travel in a rotating helical path. Neutrons that are either too fast or too slow get absorbed. Only neutrons with the right velocities are transmitted thereby transforming a white incident neutron spectral distribution into a monochromated distribution with mean wavelength λ and wavelength spread (FWHM) $\Delta\lambda$. Velocity selectors are either of the solid drum type (with helical slot) or of the multidisk type.

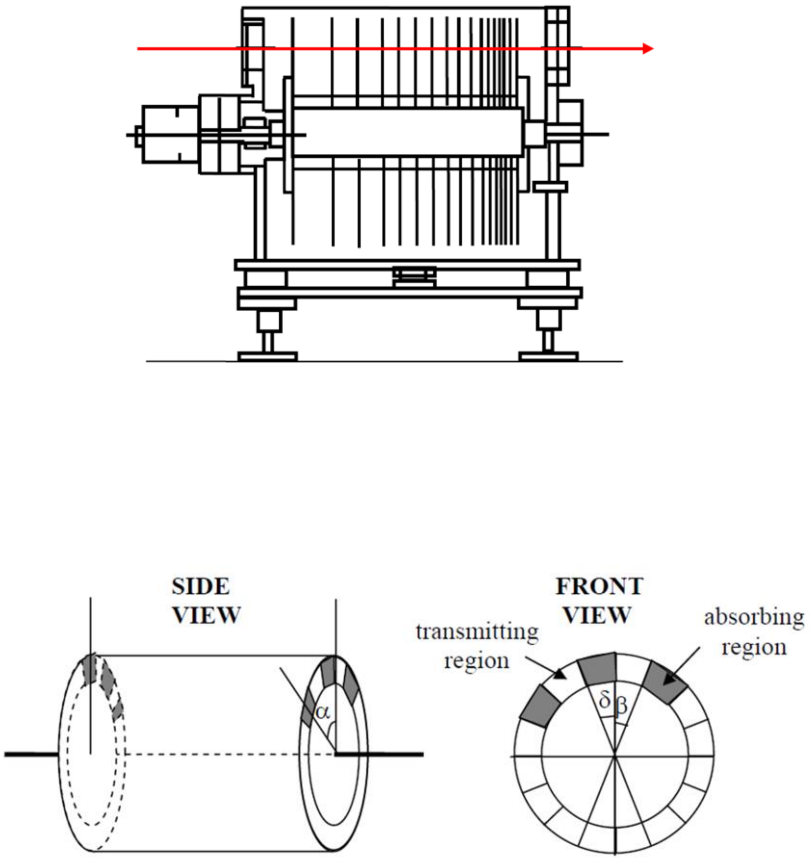

Fig. 3.5 Schematic representation of a multi-disk velocity selector. A white neutron spectrum is incident from the left and a monochromated beam is transmitted toward the right. Changing the rotation speed changes the neutron wavelength. Tilting the selector horizontally changes the wavelength spread. Magnetic coupling is used to drive the selector rotation to high rotation speed. Temperature and vibration sensors insure reliable operation. Schematics of a velocity selector explicitly showing three absorbing sectors and two transmitting windows between them.

Velocity selectors rotate at constant frequency ω which is varied to change the transmitted neutron wavelength λ. A typical selector has an overall length L (length of the rotating "drum") and a radius R (between the selector rotation axis and the neutron window). The helical path is characterized by a pitch angle α. This is the angle by which the selector rotates while neutrons cross its length L. Equating the time it takes for neutrons to travel that distance L to the time it takes the selector to rotate the angle α gives a relationship between the neutron wavelength λ and the rotation speed ω.

$$\lambda = \frac{\alpha h}{Lm\omega} \tag{3.2}$$

Here h is Planck's constant, and m is the neutron mass.

3.3. Sample Chamber

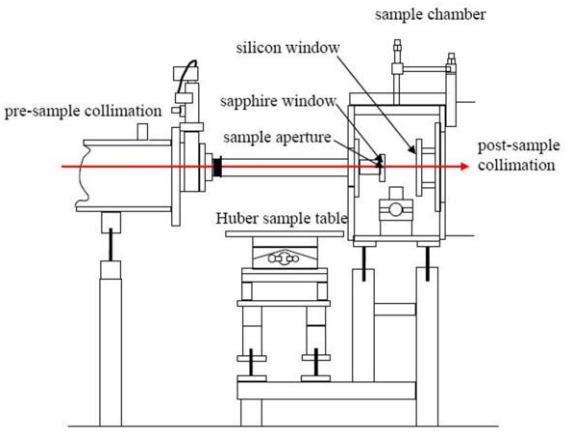

Fig. 3.6: Schematic drawing of the sample area showing the sample chamber on the right and a sample table for oversized environments on the left. Two gate valves are used to isolate the evacuated areas (pre-sample and post-sample flight path) when pumping down or evacuating the sample chamber. This softens the shock on the brittle neutron windows during such rapid pressure surges.

The sample chamber usually contains a translation frame that can hold many samples. Heating and cooling of samples (-10 ^{o}C to 200 ^{o}C) as well as other sample environments (cryostats, electromagnets, ovens, shearing devices, etc) are often accommodated. The oversized sample environments are mounted on a 22” diameter Huber sample table instead. This sample table can be rotated around a vertical axis and translated in and out of the neutron beam. This translation is useful for moving the in-situ Couette shear lead shield linear actuator neutron guide aperture empty beam position movable table cell (for example) from the radial position to the tangential position.

3.4. Post Sample Flight Path

The post sample flight path is usually an evacuated cylindrical tube (to avoid scattering from nitrogen in air) that permits the translation of an area detector along rails in order to change the sample-to-detector distance.

3.5. Area Detector

Two-dimensional area detectors are essential components for SANS instruments. The position sensitive detection is achieved in one of two ways. (1) Delay line detectors sense the position of the detection event through the time delay at both ends of each cathode. Only two winding cathodes wires (one for X and one for Y positioning) are used. (2) The other (and most used) detection scheme uses the coincidence method whereby only X and Y events that arrive in time coincidence are counted. This last method uses 128 wires for X and 128 wires for Y cathodes and can handle higher count rates.

The area detector is often a gas detector with 0.5 cm to 1 cm resolution and typically 128*128 cells. The detection electronics chain starts with preamplifiers on the back of the detector and comprises amplifiers, coincidence and timing units, plus encoding modules and a means of histogramming the data and mapping them onto computer memory. In order to avoid extensive use of vacuum feedthroughs, high count rate area detector design incorporates most electronics modules (amplification, coincidence, encoding, etc) inside an electronics chamber located on the back of the detector. In this design, flexible hoses are, however, needed to ventilate the electronics and to carry the high voltage and powering cables in and the encoded signal out.

Most neutron area detectors use 3He as the detection gas that undergoes the following nuclear reaction:

$$^{1}n_{0} + {}^{3}He_{2} \rightarrow {}^{1}H_{1} + {}^{3}H_{1} + 765\ keV \qquad (3.3)$$

The reaction products consist of two charged particles: a proton ($^{1}H_{1}$) and a triton ($^{3}H_{1}$) released in opposite directions with a combined kinetic energy of 765 keV. This kinetic energy is dissipated by ionization of the proportional counting gas (CF4 mostly). Since the incident neutron kinetic energy is very small (1/40 eV for thermal neutrons), thermal neutron detectors cannot measure neutron energies; they can only detect neutron positions. The released charged particles are attracted by the anode plane high voltage and liberate electrons. These are accelerated towards the anodes and therefore create a detection cloud through secondary ionization (charge multiplication). The two cathode planes (for detection in X and Y) are located on both sides of the anode and are kept at a low bias voltage in order to increase detection behind the cathodes. The detection cloud which is created close to the anode induces a charge on the closest cathodes (through capacitive coupling) which can be sensed by the charge sensitive preamplifiers. An X-Y coincidence pair is then selected and processed as real event.

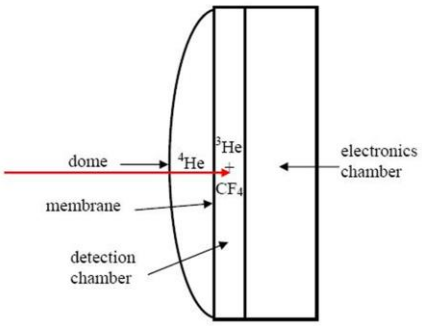

Fig. 3.7: Schematic representation of a neutron area detector.

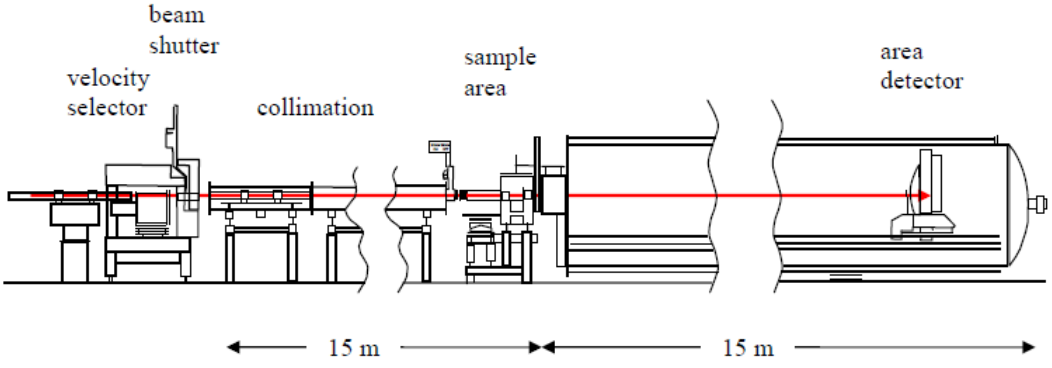

Fig 3.8 Schematics of a 30m SANS instrument at NIST

Reference

[1] B. Hammouda, “SANS from Polymers Tutorial”, NIST Center for Neutron Research Report (1995)

[2] https://en.wikipedia.org/wiki/Neutron

[3] For example, see, R. Von Flatern, “Paraffins: The scourge of deepwater development,”. Offshore 57, N3, 28-31 (1997).

[4]. http://www.pipetechamericas.com/ Pipe Tech America Summit 2010.

[5] R. Tao and X. Xu, “Reducing the viscosity of crude oil by pulsed electric or magnetic field,” *Energy & Fuels*, **20,** 2046-2051 (2006).

[6] R. Tao, “The Physical Mechanism to Reduce Viscosity of Liquid Suspensions,” International J. of Modern Physics B, V. 21, N28&29, pp. 4767-4773 (2007).

CHAPTER 4

SANS VISUALIZATION OF ELECTRIC RHEOLOGICAL CHANGE

According to Dr. Tao`s Rheology Theory, an electric field can aggregate the suspended nano-particles inside crude oil into short chains along the field direction, which will break the symmetry, making the viscosity anisotropic; along the field direction, the viscosity is significantly reduced. [1][2][3]

Compared to the conventional heating method, this technology consumes much less energy and is much faster and, therefore, much more efficient. The work has received great general interest for its impact on energy production and transportation.[4] The technology is developing very fast. Rocky Mountain Oilfield Testing Centre (RMOTC) of Department of Energy recently published three reports, showing that the field tests have confirmed that this new technology is energy efficient and feasible on pipelines.[5-7] The TransCanada Keystone project recently decides to try this technology for its pipeline. These speedy developments urge us to resolve some controversy in the area quickly and clarify many important questions about the underlying physics.

Crude oil is a liquid suspension. The base liquid, consisting of gasoline, kerosene, and diesel, has a dielectric constant lower than that of the suspended particles, such as asphalt particles, paraffin particles and sulfur particles, etc. The proposed basic physics of the new technology is illustrated in Fig. 4.1. When a strong electric field is applied along the flow direction in a small section of the pipeline, the suspended particles are polarized by the electric field. The dipolar interactions quickly aggregate the particles into short

chains along the field direction. Under such a condition, the space symmetry is broken. Similar to the flow of nematic liquid crystal with its molecule alignment in one direction, the viscosity is no longer isotropic.[4] Along the axial direction, viscosity is down to the minimum as these aggregates are streamlined along the flow direction with a very low intrinsic viscosity. Hence the crude oil flow inside the pipeline is greatly enhanced.

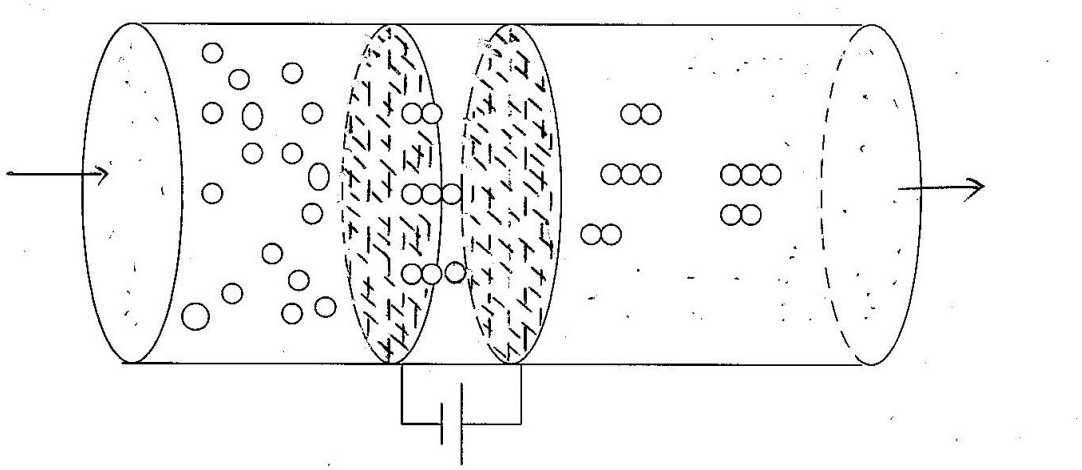

Fig. 4.1 As the crude oil flow passes a strong local electric field, the suspended particles aggregate along the field direction, and the viscosity along the flow direction is reduced.

However, the theoretical prediction that the applied electric field could aggregate suspended particles inside crude oil was not obvious. The issue was controversial. For example, I. N. Evdokinov and K. A. Kornishin in 2009 claimed that magnetic field and electric field cannot aggregate particles inside crude oil.[5] In the area of electrorheological (ER) fluids, it was well established that a strong electric field aggregates the suspended dielectric particles of micrometer size into chains and chain-

based thick columns, which are close packed and have the body-centered tetragonal (BCT) lattice structure.[6-8] Similar electric-field induced aggregations have been observed in colloidal suspensions with particles in micrometer or sub-micrometer size.[13] It is also straightforward to show that at a sufficiently strong electric field, the interaction between induced dipole and local electric field inside crude oil is stronger than the thermal motion, leading to the particle aggregation. The controversy comes from a simple fact that crude oil is very dark and the suspended particles inside crude oil, such as paraffin particles, are typically of nanoscale size; they cannot be observed under a microscope or with conventional optical devices. In fact, we even did not succeed in using x-ray or TEM to monitor the suspended particles inside the crude oil. To resolve this outstanding issue, which is also the key for the new technology, we must have some direct evidence to show that an electric field induces particle aggregation inside crude oil. For this purpose, we carried out neutron scattering studies at the NIST Center for Neutron Research (NCNR).

4.1 Experimental Setup

This 30 meter long SANS instrument is ideal for our experiment. Jointly developed and sponsored by NCNR, ExxonMobil Research and Engineering Co., and University of Minnesota, the instrument has undergone a number of improvements over the years. The improvements, including a higher resolution 2D detector and focusing refractive lenses, have extended the Q-range of the instrument which now goes from 0.008 nm^{-1} to 7.0 nm^{-1} to enable structural features in materials ranging from roughly 1 nm to over 500 nm to be probed.

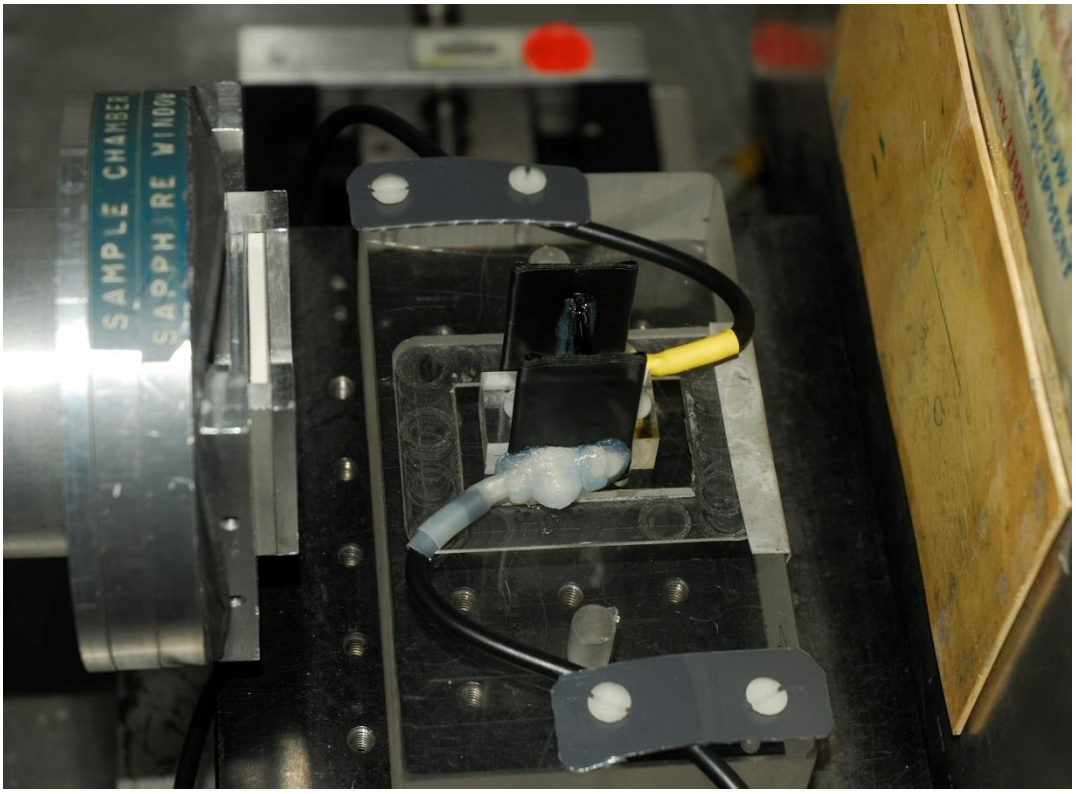

Fig. 4.2 crude oil sample is in a special capacitor, consisting of two pieces of cadmium as electrodes and two pieces of quartz glass as windows. The neutron beam passes through the quartz windows and the crude oil sample and comes to the detector.

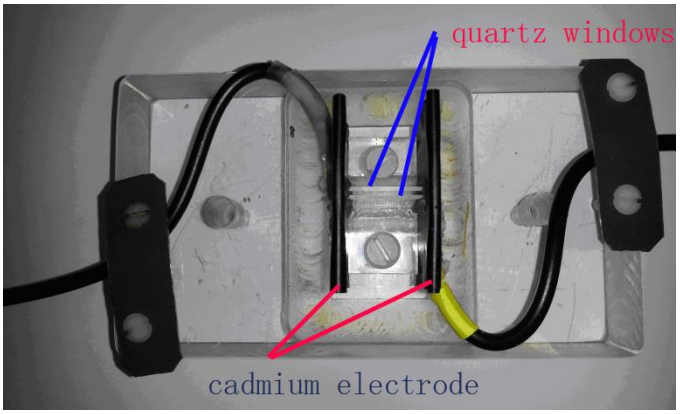

Fig. 4.3 A high voltage can be applied to cadmium electrodes to produce an electric field perpendicular to the neutron beam.

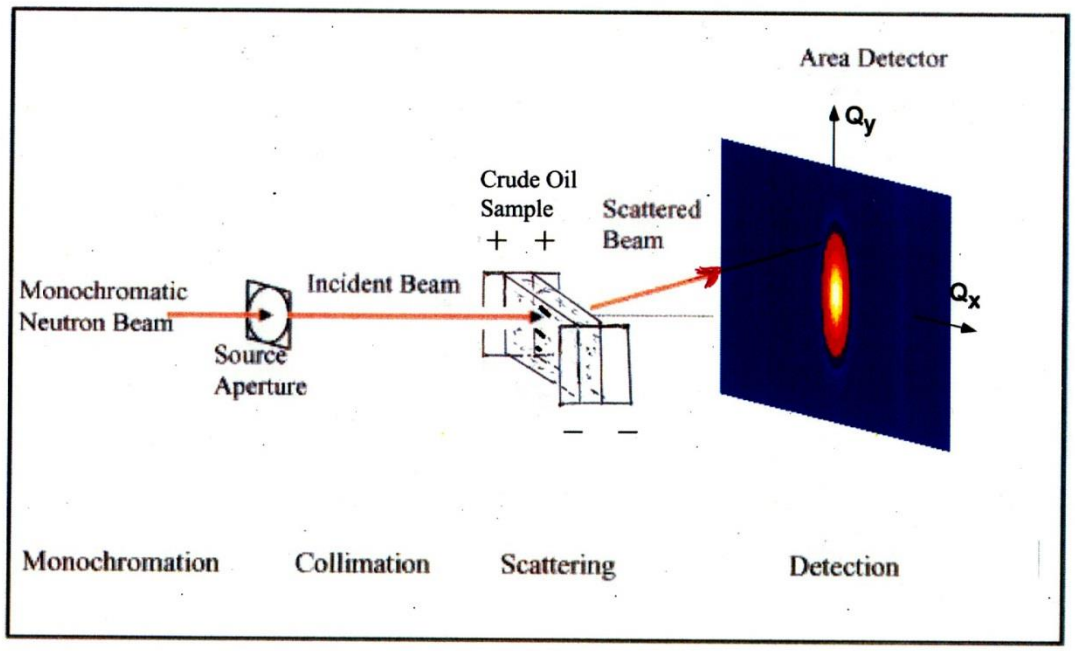

Fig.4.4 The outline of set up for the neutron scattering experiment.

Our crude oil sample is in a special capacitor, consisting of two pieces of cadmium as electrodes and two pieces of quartz glass as windows (Fig.4.2 4.3). The neutron beam

passes through the quartz windows and the crude oil sample and comes to the detector (Fig. 4.4).

A high voltage can be applied to the cadmium electrodes to produce an electric field perpendicular to the neutron beam. We select cadmium for our electrodes because cadmium is a good neutron absorber, which reduces the neutron scattering noise and blocks the large angle scattering.

Our tests were mainly with a light paraffin base crude oil sample (API 34) because the paraffin base crude oil is the controversial one. In 2006, it was also reported that magnetic field might be useful to reduce viscosity of paraffin base crude oil but had almost no effect on asphalt base crude oil.[1] However, the experiments by a Brazil group in 2011 showed that magnetic field has an effect for some kinds of paraffin base crude oil, but has little effect on other kinds of paraffin base crude oil.[10] This is related to the paraffin molecule structure: If the molecule has a ring structure, the paraffin is diamagnetic; then, similar to electric field, a strong magnetic field in the flow direction can aggregate paraffin particles into short chains to reduce the viscosity along the flow direction. If the paraffin molecule's hydrocarbon chain has no ring structure, the paraffin is not sensitive to a magnetic field, then the magnetic field basically has no effect on the crude oil. This finding indicates that in order to reduce the crude oil viscosity, we have to rely on the electric field for all kinds of crude oils, including paraffin base crude oil. Therefore, it is crucial to see if our neutron scattering experiment could verify the electric field induced particle aggregation inside paraffin base crude oil. Some tests with a heavy asphalt base crude oil (API 21) were also carried out in spite of the fact that the electric field aggregates asphalt particles inside crude oil is more established.[1]

In ER fluids, after a strong electric field is applied, the suspended particles quickly form chains and the chains aggregate into thick columns. The whole process only takes a couple of milliseconds. This quick transition can be explained as follows. When the dipoles aggregate into chains or chain-based columns, the total energy U(N) is negative and the energy per particle *U(N)/N* is more negative as N increases initially.[6] As the probability to have such structure of *N* aggregated particles is proportional to $\exp[-U(N)/k_BT]$, the aggregation is accelerated as *N* increases. The aggregated structure is more stable if it has more particles. For this reason, once the electric field is applied, many thick columns are formed quickly. If the final equilibrium can be reached, the ideal state should have all particles aggregated into one thick column, body-centered tetragonal lattice. In reality, in most cases we are unable to reach such ideal state, but we always see many stable thick columns quickly.

While the field induced dipolar interaction in crude oil is not as strong as that in ER fluids, the basic physics remains the same. Therefore, once the electric field is applied, the aggregation into chains or chain-based columns is accelerated as more particles get together. We should have sizable chains and chain-based columns quickly because the aggregated structure is more stable if it has more particles. This aggregation has been verified by our neutron scattering experiment.

Our test procedure was as follows: We first obtained the neutron scattering pattern without electric field applied. Afterwards, we turned on the electric field and gradually increased the field strength. When the suspended particles inside the crude oil were aggregated into structures by the electric field, the neutron scattering patterns changed. Hence, not only our theoretical prediction was verified, but the pattern itself also

provided us with the information about the size and shape of the aggregated chains. Based on this information, we can calculate the viscosity reduction, further confirming our field tests. [10-13]

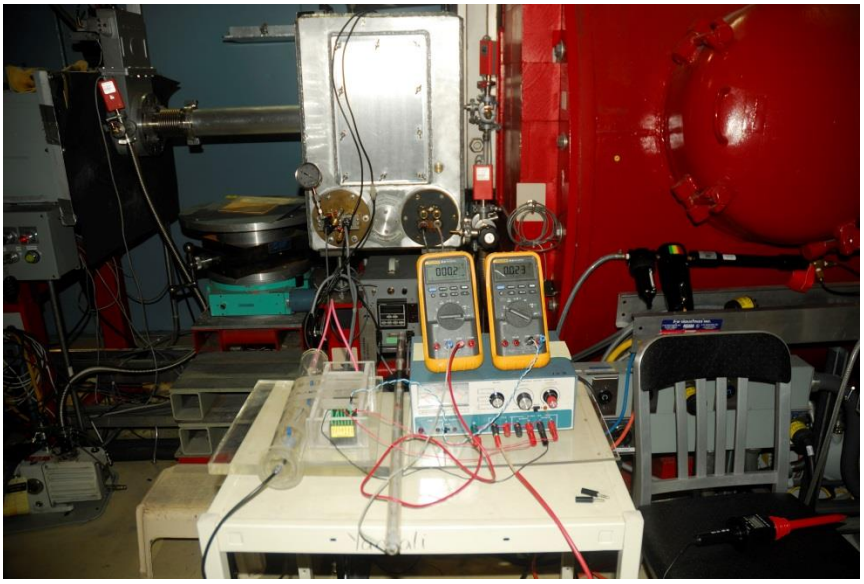

Fig.4.5 High voltage tiny current power supply system.

Fig.4.6 Changing crude oil sample and applying different voltage

4.2 Data Reduction

We use IGRO Pro to reduce the data, Fig. 4.7 is a raw data display. 2-D SANS data is displayed versus detector pixel (left and bottom axes) and versus Qx and Qy (top and right axes), along with a color scale. Important information about the data is displayed at the top of the graph, including the filename, the (X, Y) position of the cursor, and the count value. The horizontal, vertical, and total q-values (in Angstroms^{-1}) are also displayed. Further information about the file can be displayed by clicking the "Status" button, and the information is printed to the command window at the bottom of the screen. The color mapping of the detector counts can be toggled between logarithmic and linear scale by clicking the "isLin" button. The current label on the button, either "isLog" or "isLin" gives the current scaling. The displayed data can be averaged (without doing any reduction steps) by clicking the "I vs. q" button. This will present a new panel with the Average Options. For averages of sectors or slices of the 2D dataset, the region to be averaged is marked on the dataset in response to the angles and widths chosen in the panel. The defaults are for a standard circular average of the full dataset. The Color Map sliders can be adjusted as desired to alter the color display of the data.

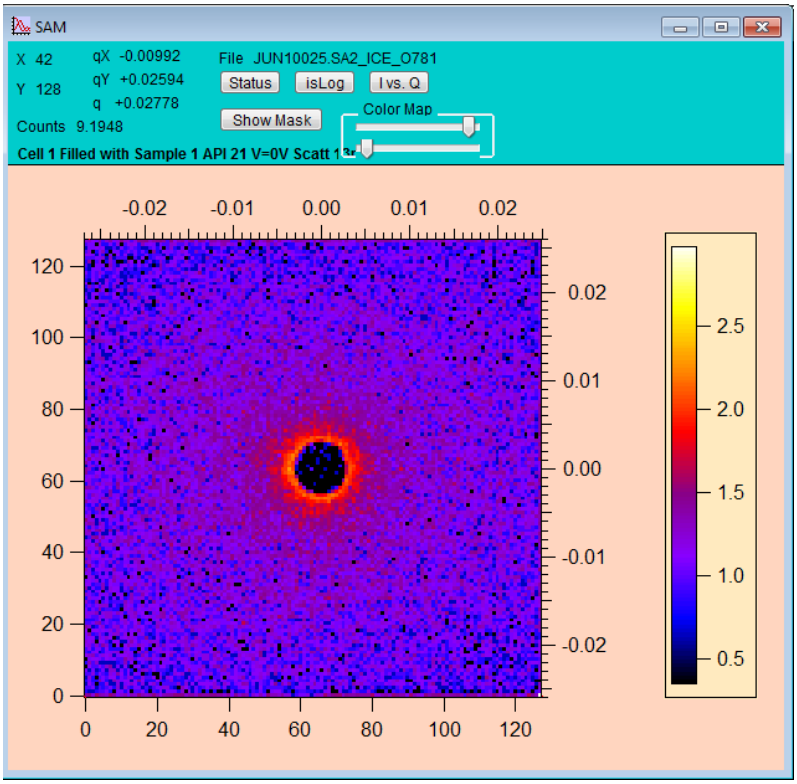

Fig. 4.7 2-D SANS data is displayed versus detector pixel (left and bottom axes) and versus Qx and Qy (top and right axes), along with a color scale. The Color Map sliders can be adjusted as desired to alter the color display of the data.

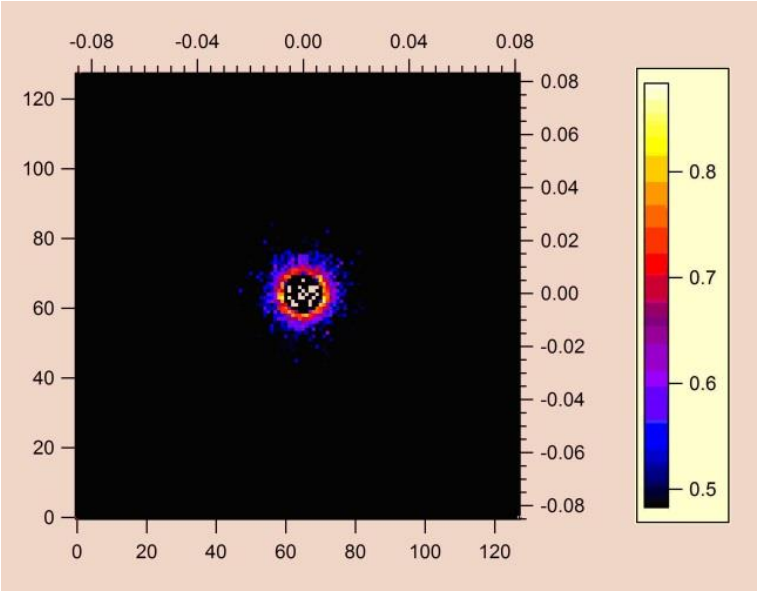

Fig. 4.8 The neutron scattering pattern without electric field applied

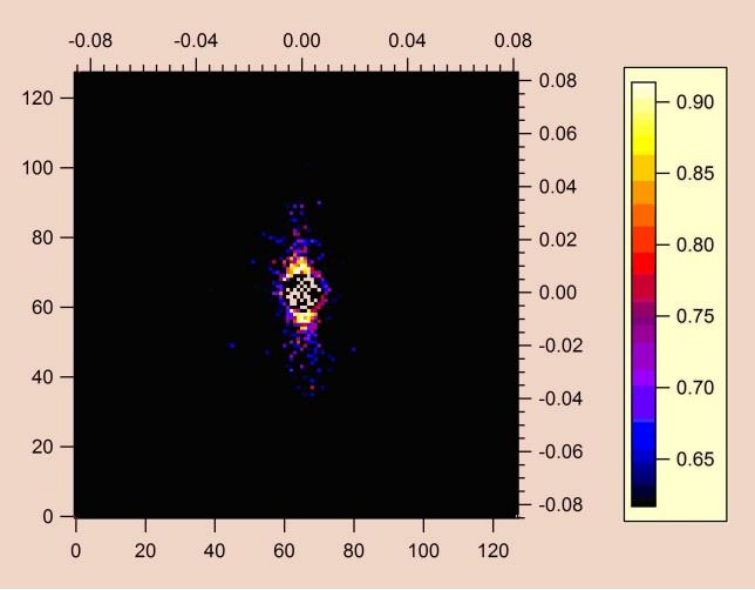

Fig.4.9 The neutron scattering pattern with electric field applied E=250V/mm

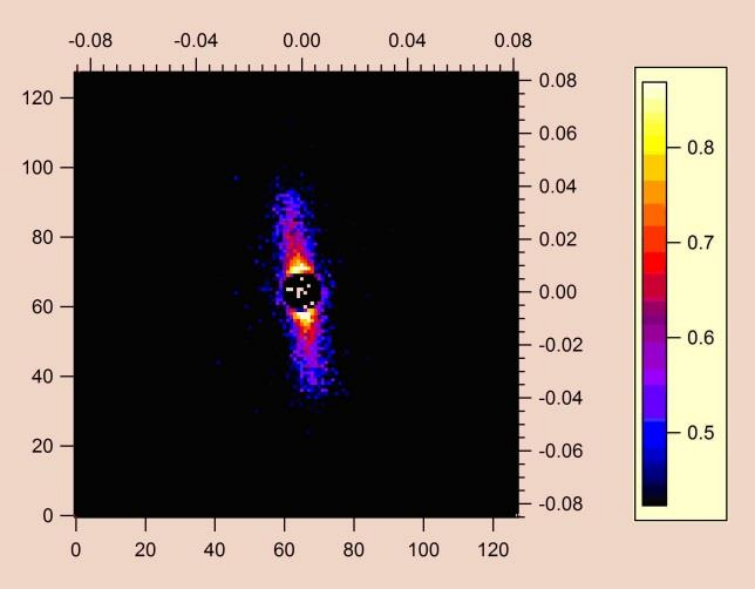

Fig.4.10 The neutron scattering pattern with electric field applied E=400V/mm

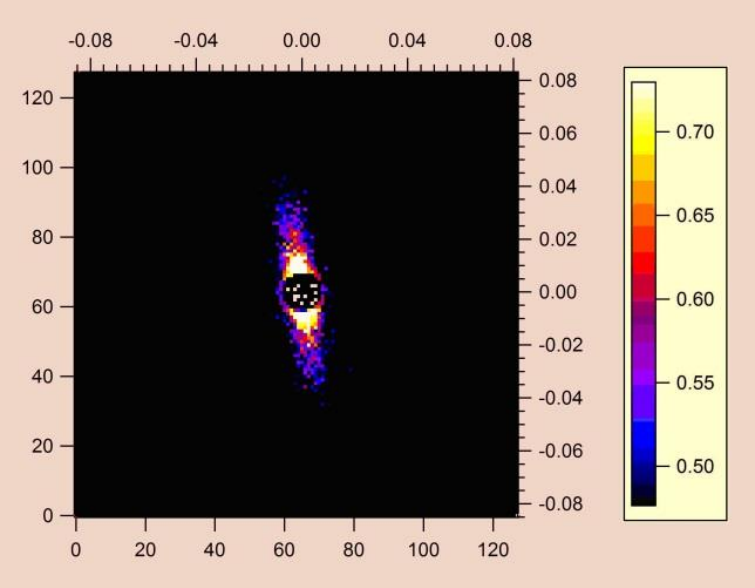

Fig. 4.11 The neutron scattering pattern with electric field applied E=750V/mm

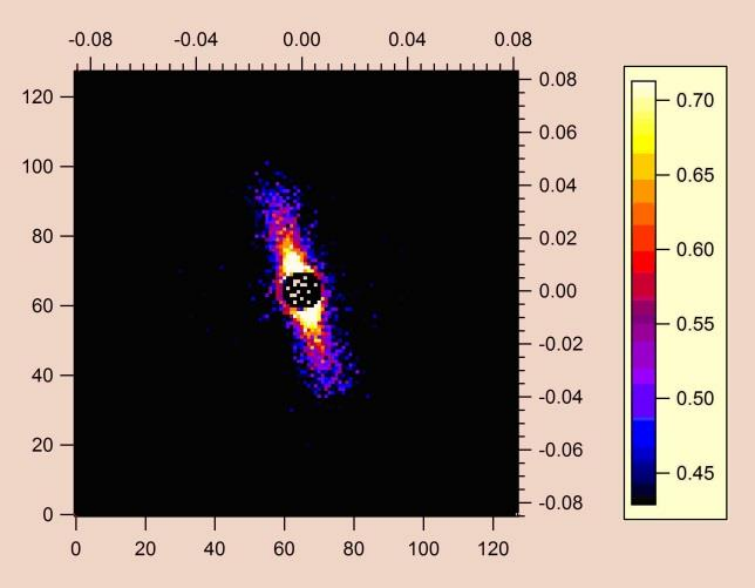

Fig. 4.12 The neutron scattering pattern with electric field applied E=1100V/mm

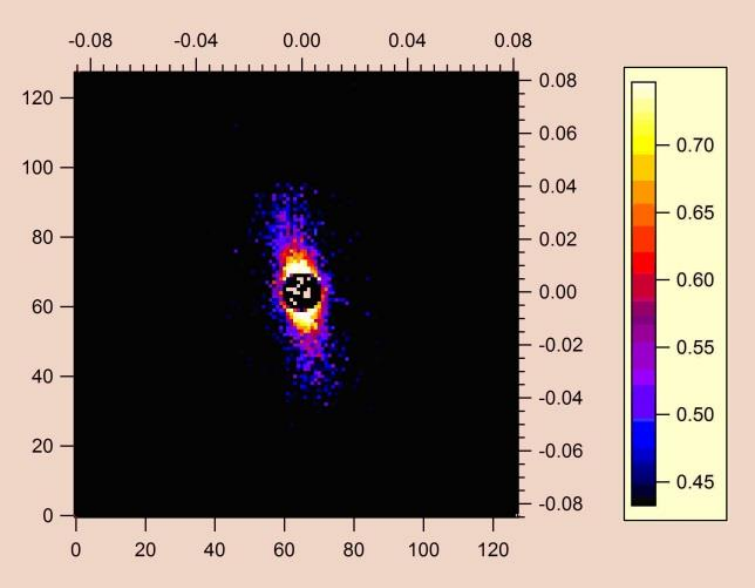

Fig. 4.13 The neutron scattering pattern with electric field applied E=1500V/mm

With these neutron scattering patterns, it is not difficult to confirm the theoretical prediction. And the pattern itself also provided us with the information about the size and shape of the aggregated chains. So, let`s take a close look at these patterns.

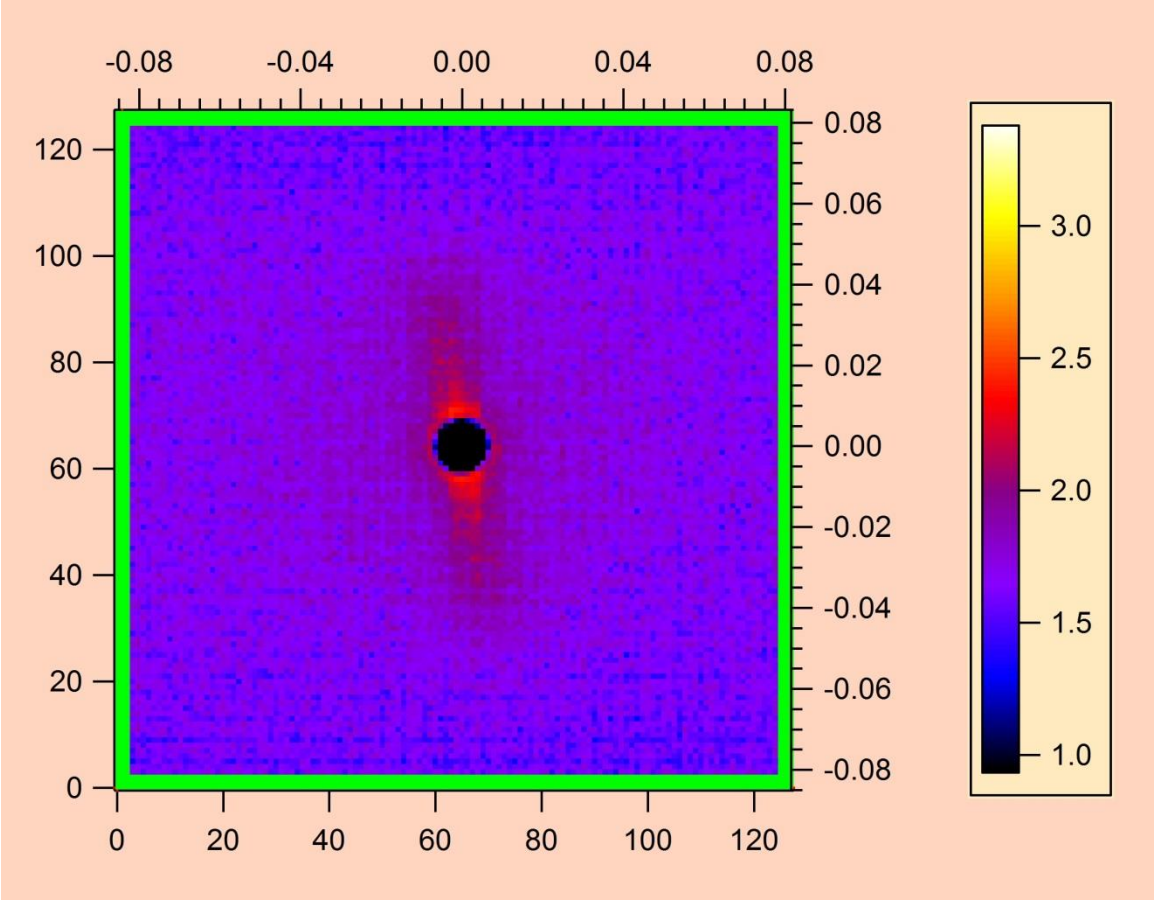

Fig. 4.14 the neutron scattering pattern raw data

We adopt SANS data reduction software IGOR Pro, which is an implementation of the VAX data reduction procedures in an easier to use, graphical interface. It is designed to work on both Macintosh and PC, and works directly on raw binary data files as collected on the VAX or through ICE.

With IGRO Pro, we can display and process 2D SANS data (subtracting background, converting to an absolute scale, averaging, etc.) and produce reduced 1D or 2D data in intensity versus wavenumber (I vs. Q).

The raw data was collected at the instruments is 2D (128 rows x 128 columns) in individually named binary files. We combined combine SAM, EMP, and BGD data to produce COR data, which was corrected for background and empty cell scattering. SAM, EMP, BGD and COR represent sample data, empty cell data, background data and sample data respectively.

The sample data is corrected for background and empty cell scattering according to the algorithm:

$$\mathrm{COR} = (\mathrm{SAM} - \mathrm{BGD}) - \frac{T_{sam}}{T_{emp}}(\mathrm{EMP} - \mathrm{BGD}) \qquad (4.1)$$

where $\mathrm{T_{sam}}$ is the transmission of the sample and $\mathrm{T_{emp}}$ is that of the empty cell.

Detector Efficiency Corrections

An important step in the data reduction process involves correcting for the detector response. The corrected data, COR, is divided, pixel-by-pixel, by the contents of DIV. This calibrated result is written to a separate work folder, CAL. A data set can be corrected for non-uniformities in the detector efficiency by dividing the data, pixel-by-pixel, by the measured scattering from an isotropic scatterer such as plexiglass or water.

Masking the data set

The last step before averaging the data to reduce it to I vs Q form is to mask the data set. This operation has the effect of marking, or masking, specific pixels in the 2D data field that are to be ignored in the subsequent averaging process.

Averaging the data set

At this point the corrected data can be reduced to I vs Q or saved in another format. Typically, the averaging operation is used to perform either a radial, angular, sector or rectangular average (ignoring all masked pixels) of the 2D data field to reduce it

to I vs Q. The averaged data are stored in individually named ASCII (text) files. Data that have been converted to an absolute scale are, after averaging, stored in a file with the extension .ABS; otherwise, the results are stored in a file with the extension .AVE. The final averaging step can also be set to save the reduced data in a 2D ASCII format. The 2D ASCII format can be re-read into the SANS Reduction package for further processing.

Once data are reduced to I vs. Q form, various types of linearized fits can be performed. See Fit Lines to Your Data for details.

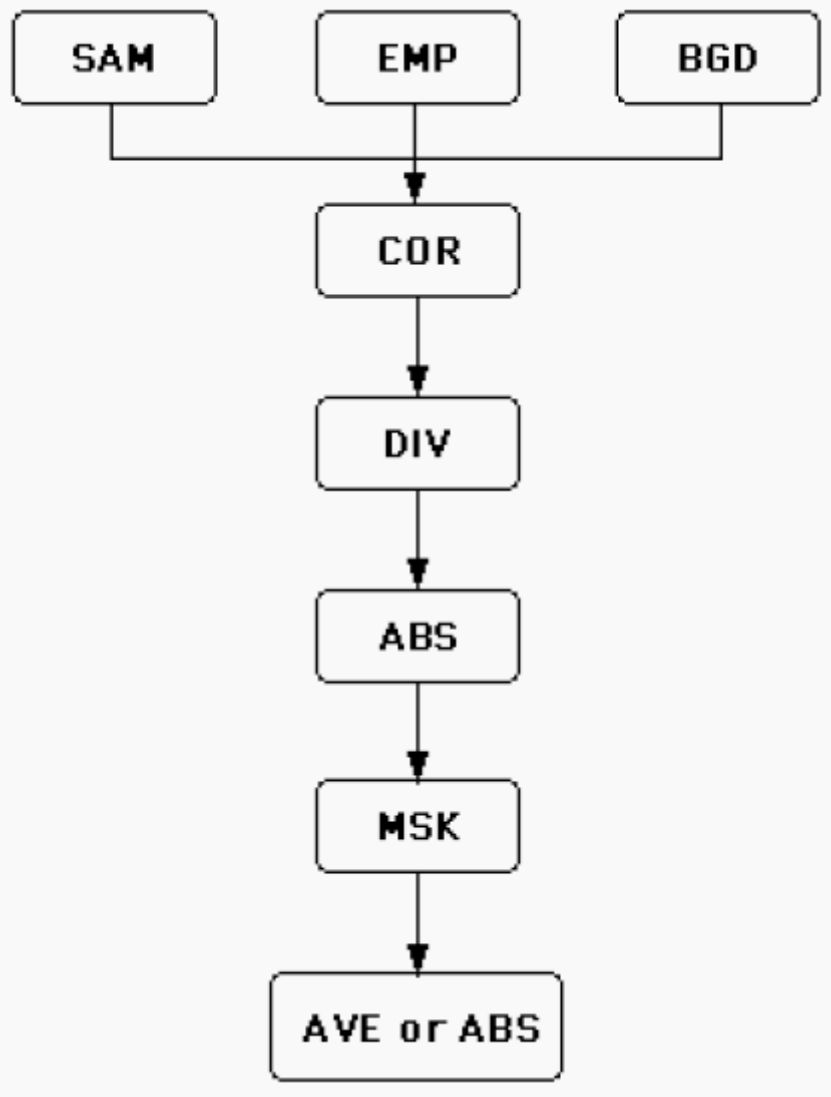

Fig. 4.15 SANS data reduction process

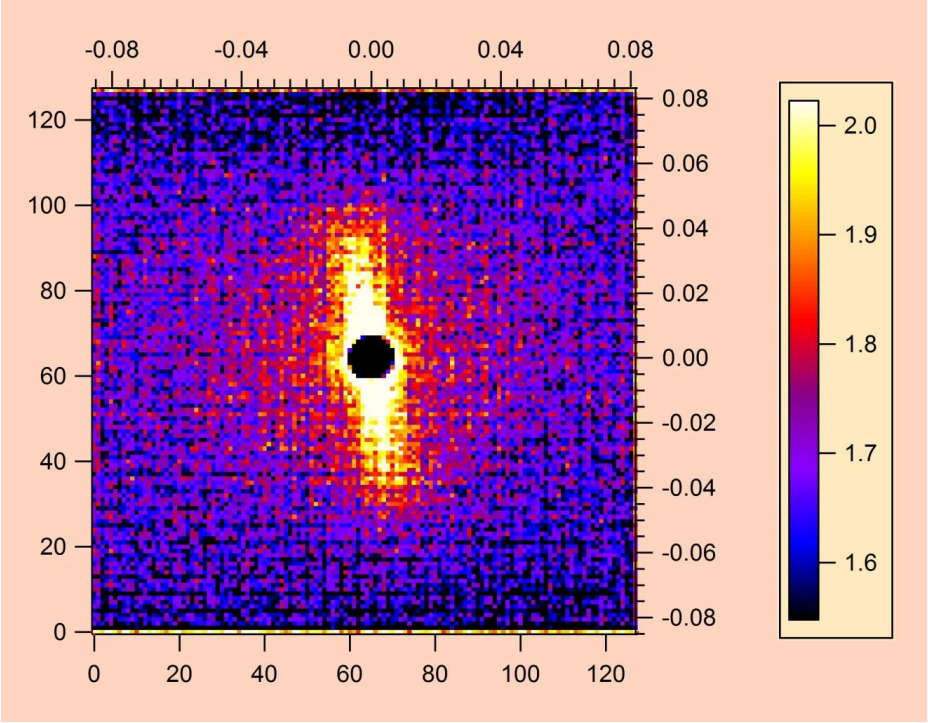

Fig. 4.16 IGRO Pro 2D RAW data display

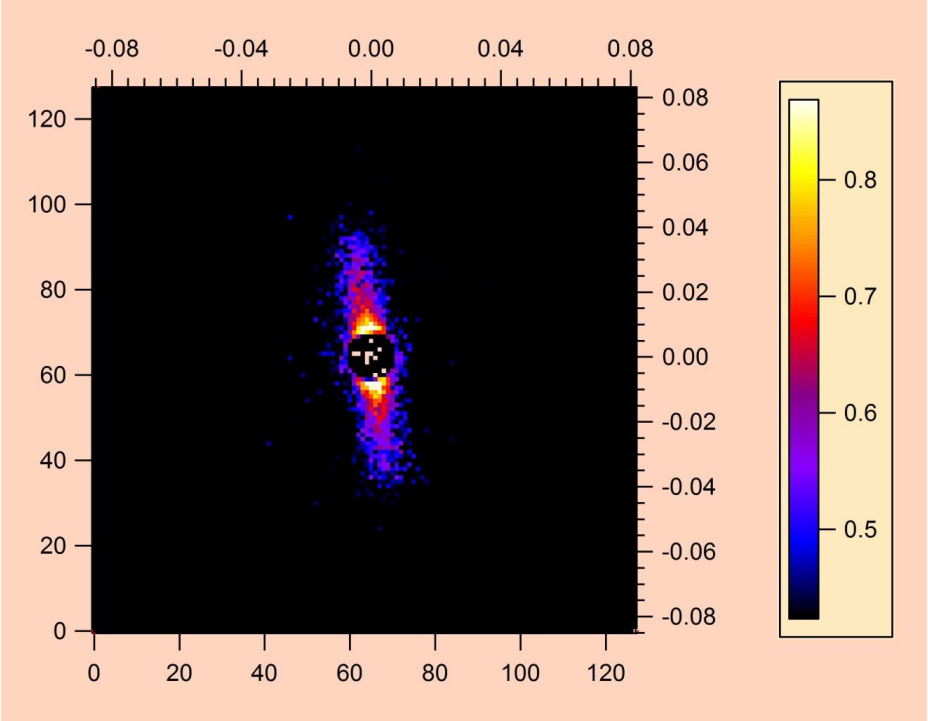

Fig. 4.17 IGRO Pro 2D reduce data display

4.3 Visualization of Electric Rheological Changing

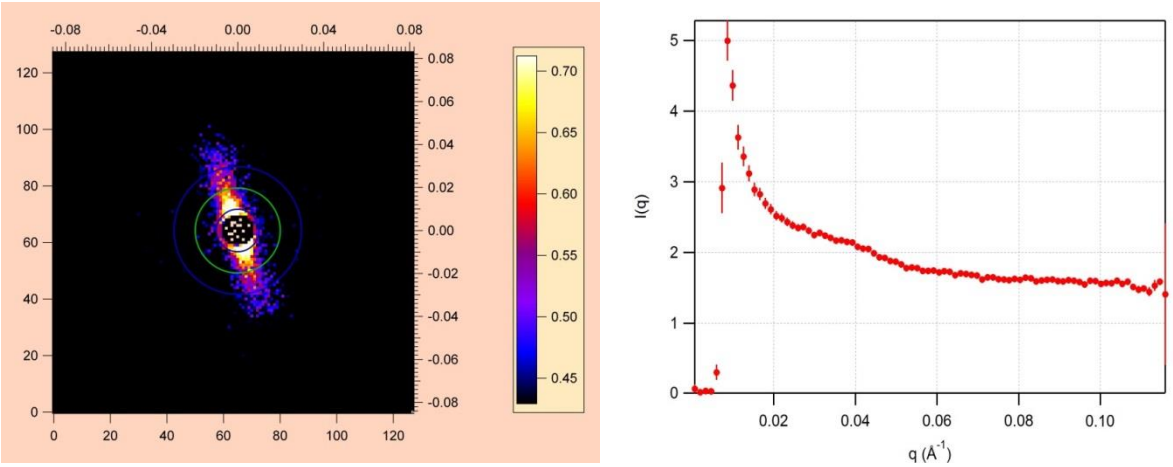

Fig. 4.18 IGRO Pro reduce data I(q) VS. q(A^{-1}) and 2D display with annular average. The corresponding Display shows what data will be included. The green line is the center of the average and the blue lines are maximum or minimum of the circular.

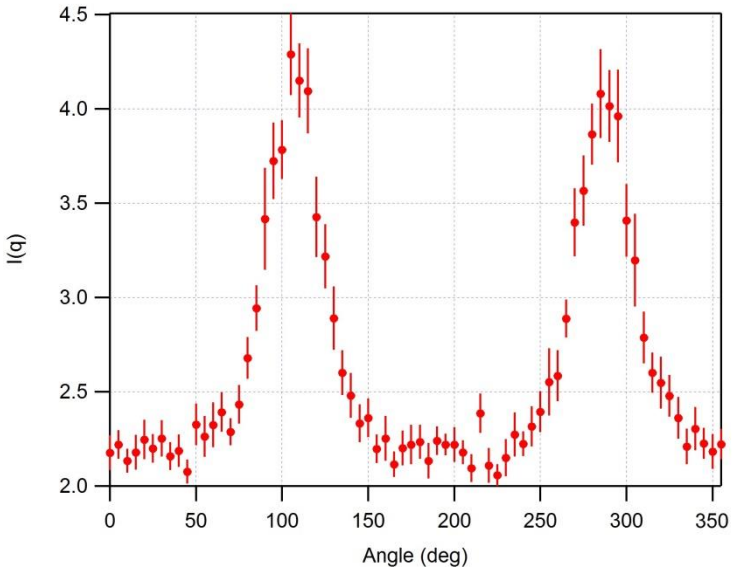

Fig. 4.19 annular average plot with two peak intensity distribution

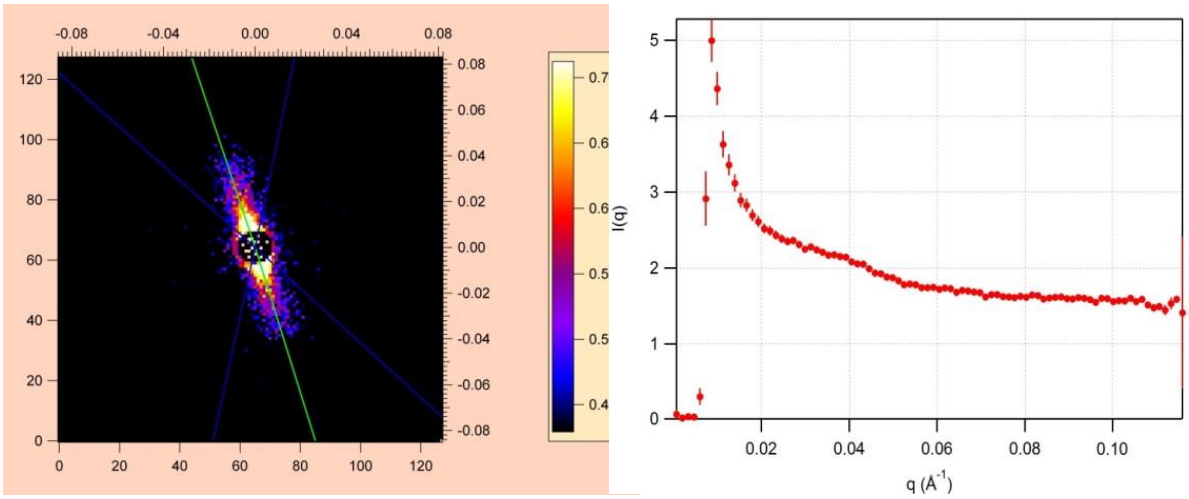

Fig. 4.20 13 IGRO Pro reduce data I(q) VS. q(A^{-1}) and 2D display with sector data reduction.

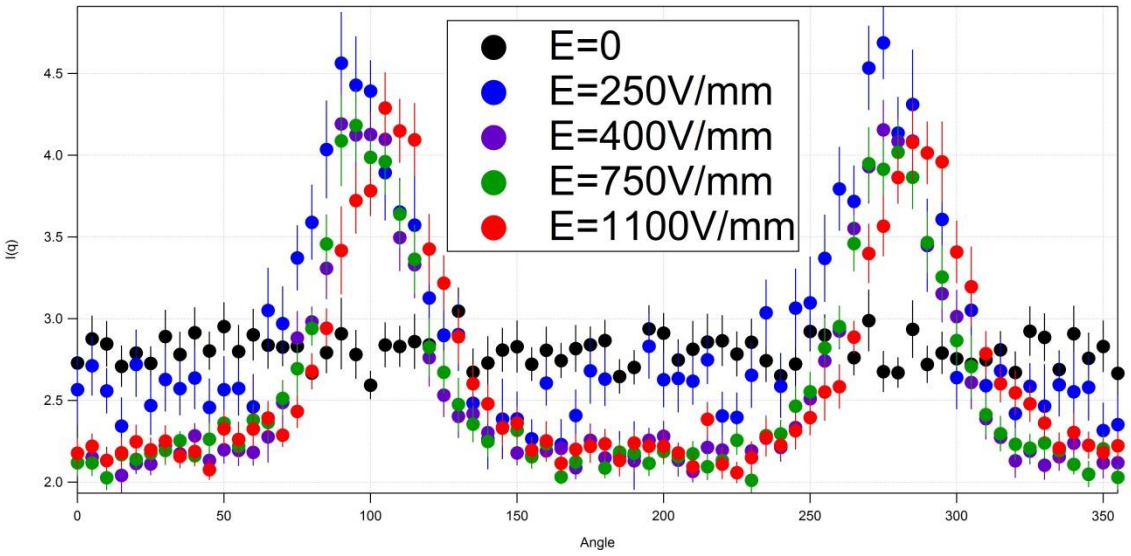

Fig. 4.21 Intensity distribution with E field

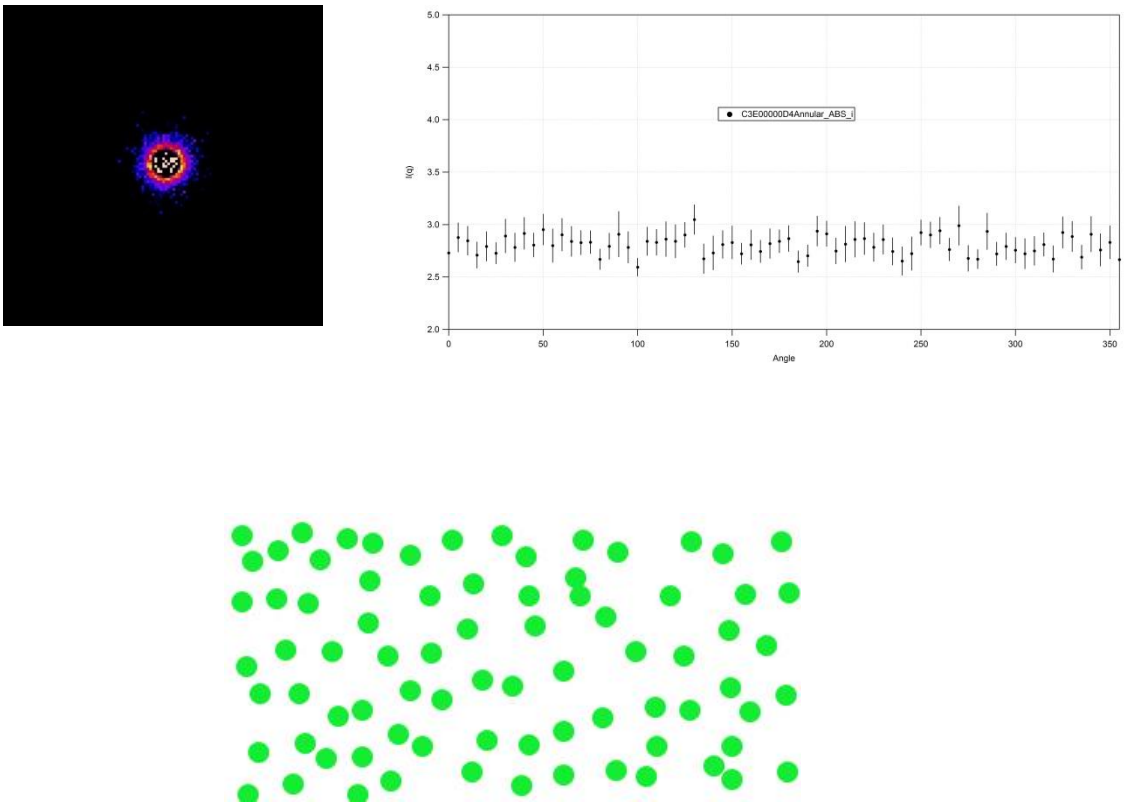

Fig. 4.22 IGRO Pro 2D display, sector average and liquid suspension of crude oil random distribution [10-13]

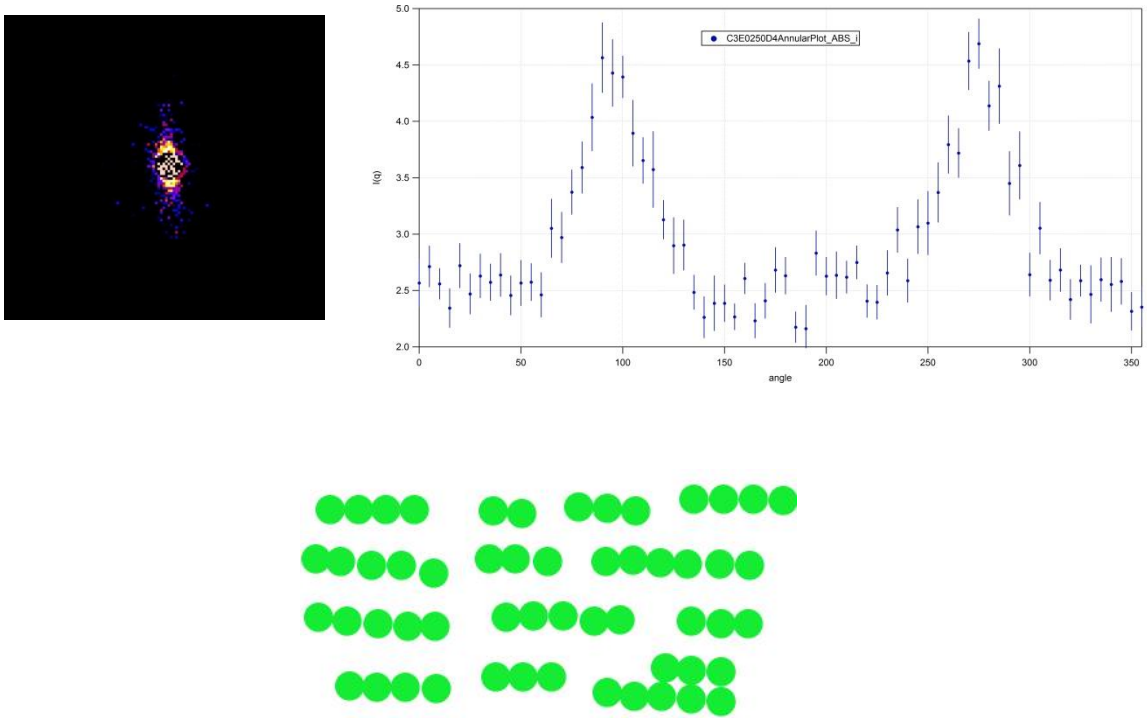

Fig. 4.23 IGRO Pro 2D display, sector average and liquid suspension of crude oil is partially aggregated [10-13]

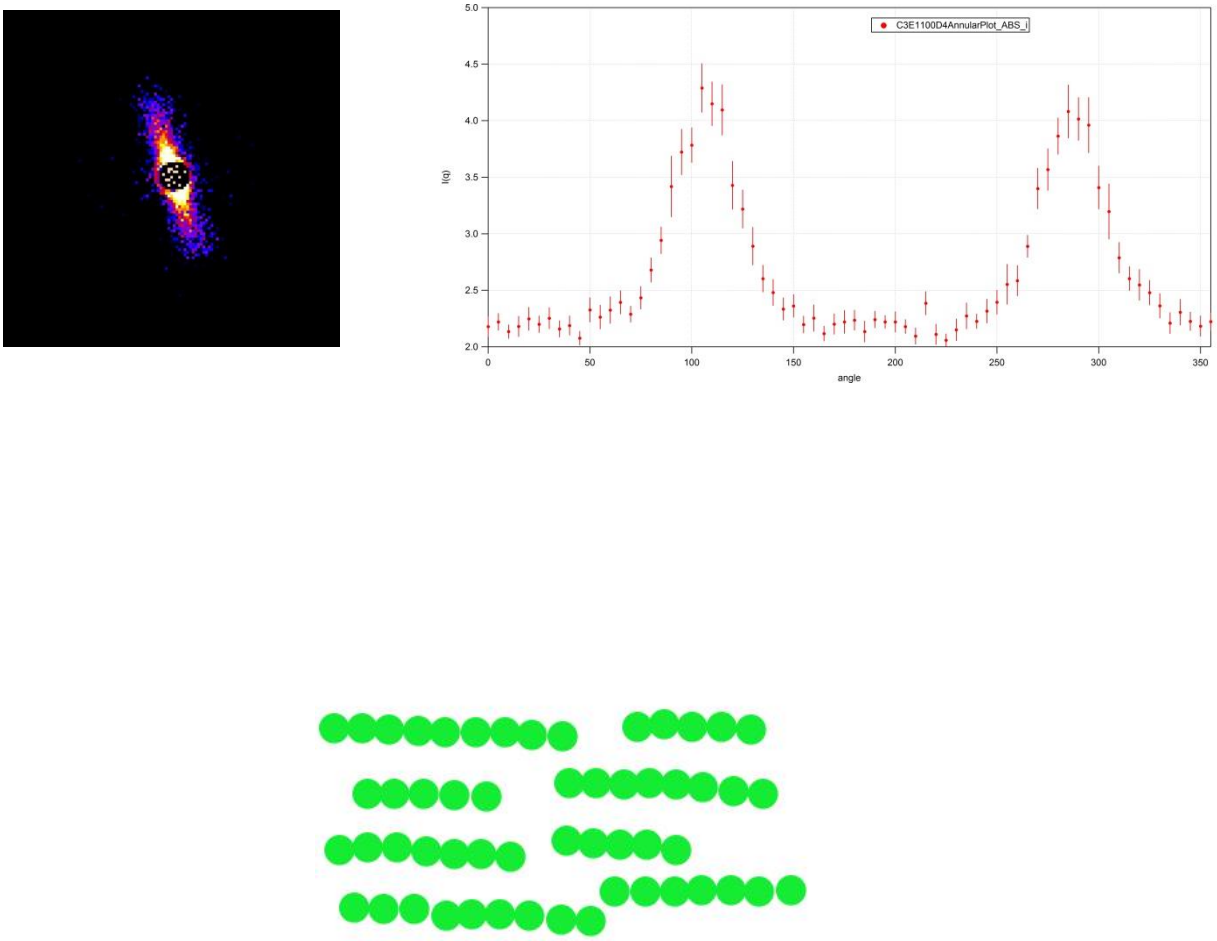

Fig. 4.24 IGRO Pro 2D display, sector average and liquid suspension of crude oil is tightly aggregated [10-13]

References

[1]Tao R. & Xu X. Reducing the viscosity of crude oil by pulsed electric or magnetic field. Energy & Fuels 2006; 20**:** 2046-2051.

[2]Tao R. Electrorheology for efficient energy production and conservation. J. of Intelligent Material Systems and Structures 2011: 22**:** 1667-1671.

[3]Tang H., Huang K. & Tao R. Electrorheology improves transportation of crude oil. J. of Intelligent Material Systems and Structures 2011; **22:** 1673-1676.

[4]Miesowicz M. The three coefficients of viscosity of anisotropic liquids. Nature 1946; 158: 27.

[5]Evdokimov I. N. & Kornishin K. A. Apparent Disaggregation of Colloids in Magneticalls Treated Crude Oil, Energy & Fuel 2009, 23, 4016-4020.

[6]Tao R. & Sun J. Three-dimensional Structure of Induced Electrorheological Solid, Phys. Rev. Lett. 1991, V67, 398-401.

[7]Chen T. J., Zitter R. N. & Tao R. Laser Diffraction Determination of the Crystalline Structure of an Electrorheological Fluid, Phys. Rev. Lett 1992, V68, 2555-2558.

[8]Tao R. & Jiang Q. Simulation of Structure Formation in an Electrorheological Fluid, Phys. Rev. Lett. 1994, V73, 205-208 .

[9]Goncalves J.L. et al. Study of the factors responsible for the rheology change of a brazilian crude oil under magnetic fields. Energy & Fuels 2011; 25: 3537-3543

[10] Du, E., Tang, H., Huang, K. and Tao, R., Reducing the viscosity of diesel fuel with electrorehological effect, Journal of Intelligent Material Systems and Structures.53, 59 (2011)

[11] Huang, K., Du, E., Tang, H. and Tao, R., Electrorheology improves E85-engine performance and efficiency, Journal of Intelligent Material Systems and Structures. 60,67 (2011)

[12] R. Tao and G. Q. Gu, Suppressing turbulence and enhancing liquid suspension flow in pipelines with electrorheology, Phys. Rev. E 91, 012304 (2015)

[13] Tao, R.; Du, E.; Tang, H.; Xu, X., Neutron scattering studies of crude oil viscosity reduction with electric field, Fuel, 134, 493,498 (2014)

CHAPTER 5

FLOW RATE LABORATORY AND FIELD TEST

5.1. Laboratory Flow Rate Testing

We tested the flow rate of our samples under several different conditions, such as low temperature. We used a U tube (Fig. 5.1) to divide the flow into two parts, one of them with E Field treatment, the other without. Comparing the flow rate, we obtained the treatment effect. The sample flow passed through two metallic meshes along a tube. A voltage was applied on these two meshes to produce a strong electric field in the space between the meshes. After an electric field was applied at the right tube, the flow rate in the right tube increased significantly. The right cup collected (34%) more bunker fuel than the left side. In the experiment, the bunker fuel took about 18.8 seconds to pass the two meshes. The current was moderate, 25μA. We also found the temperature was constant; therefore, there wasn't a temperature effect about the viscosity reduction. So the viscosity reduction was 100% due to the electric field effect.[1-7]

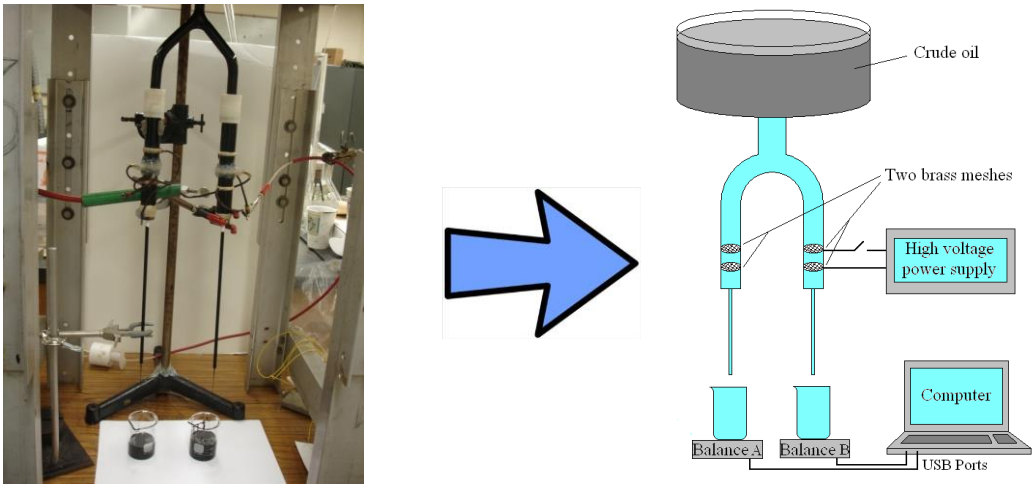

Fig. 5.1 U Tube E field treatment and flow rate measurement instrument.
There are three meshes with gap of 25mm to apply E field treatment to the bunker oil.
The capillary has a length of 270mm and a diameter of 3.625mm.

The maximum increased flow rate was 30% by electric field treatment, that is, the viscosity was reduced by at least 50%. From Fig. 5.2 we clearly see that the flow rate increased right after the treatment with E=1000V/mm. The flow increased as the electric field increased, as shown in Fig. 5.3.

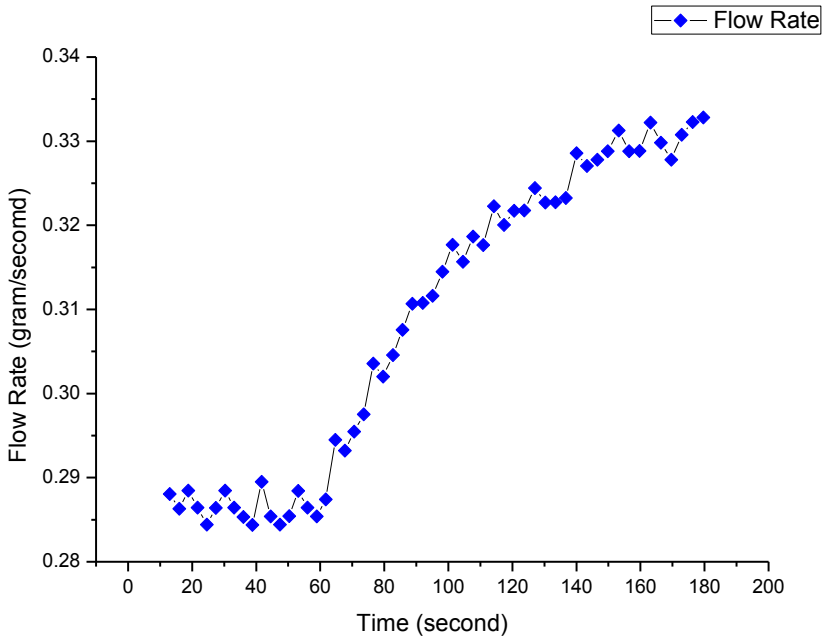

Fig. 5.2 Flow rate increase with the electric field (E=1000V/mm) increase

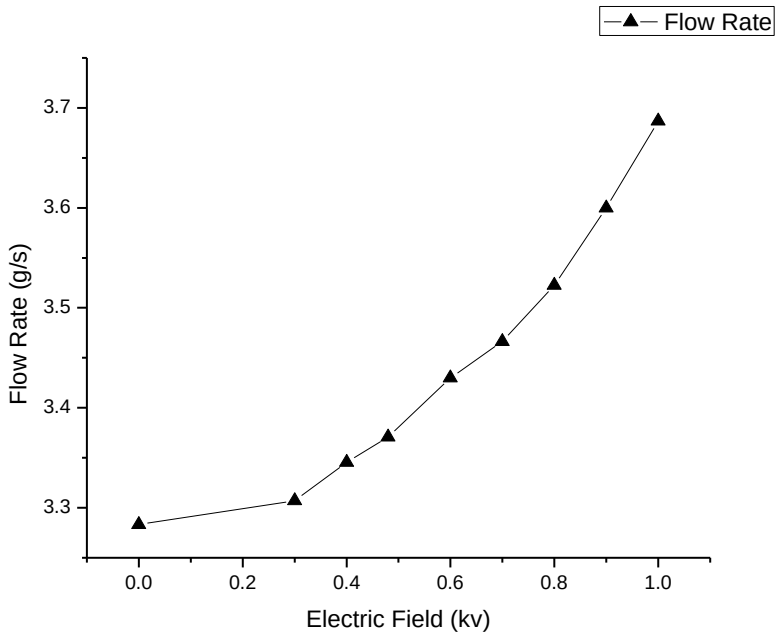

Fig. 5.3 Flow rate increase with the electric field increase

Cold weather is a big challenge to crude oil transportation via pipeline. This is because of the huge energy (i.e. high pumping power and heating) required to overcome the high-pressure drop in the pipeline due to the high viscosity at reservoir conditions.

At low temperature, our technology increases the flow rate of Daqing oil by 600%. It is 100 Times More Energy Efficient than heating. Our lab tests show that the treated oil will return to the original viscosity in more than 24 hours. [8-9]

Fig. 5.4 Low temperature Flow rate test set up

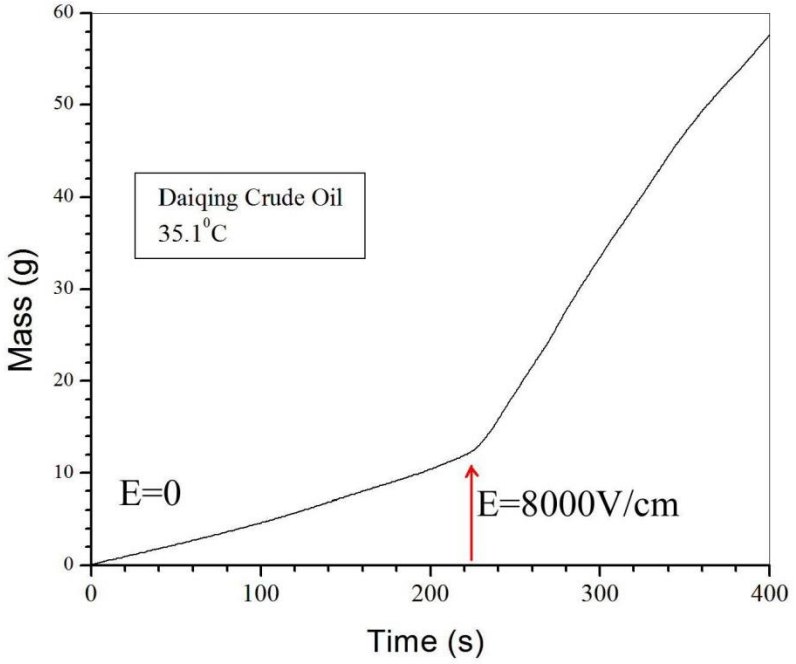

Fig. 5.5 600% increase in the flow rate (slope) of Daqing oil

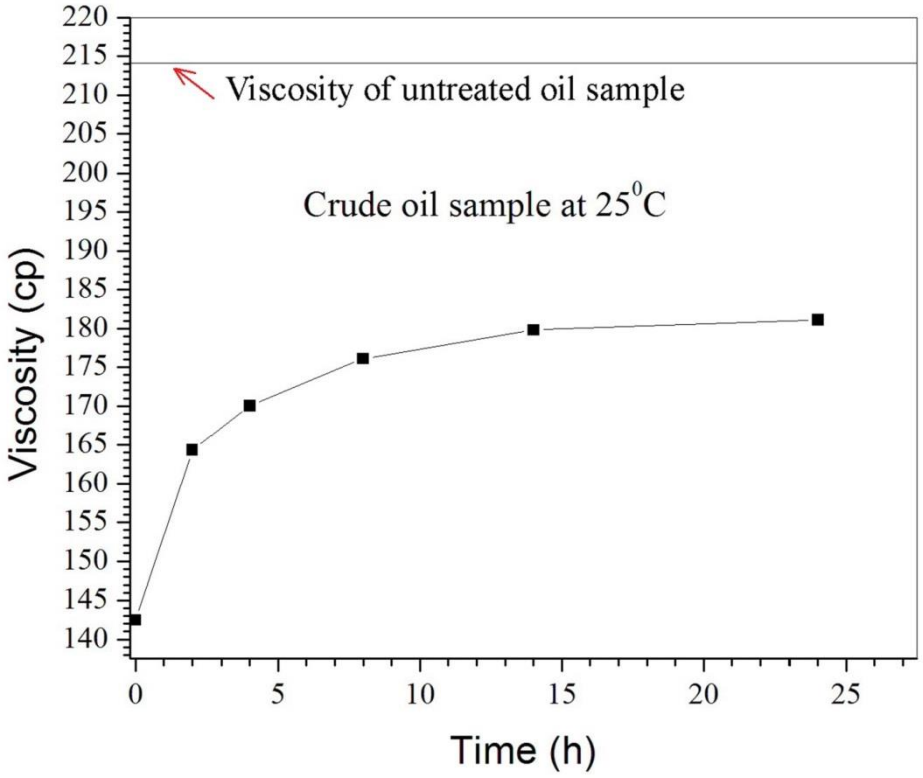

Fig. 5.6 The treated oil retains low viscosity around 24 hours

Also, there are pipeline tests, involving the DOE, Daqing field and Keystone pipelines.

5.2 Wyoming DOE Pipeline Testing[10-11]

The untreated crude oil has viscosity 81.6 cp. After the device was turned on, the treated crude oil had viscosity 48.95cp, down 40%. After the device was turned off, the untreated crude oil pushed the treated oil away and the viscosity returned to the original value.

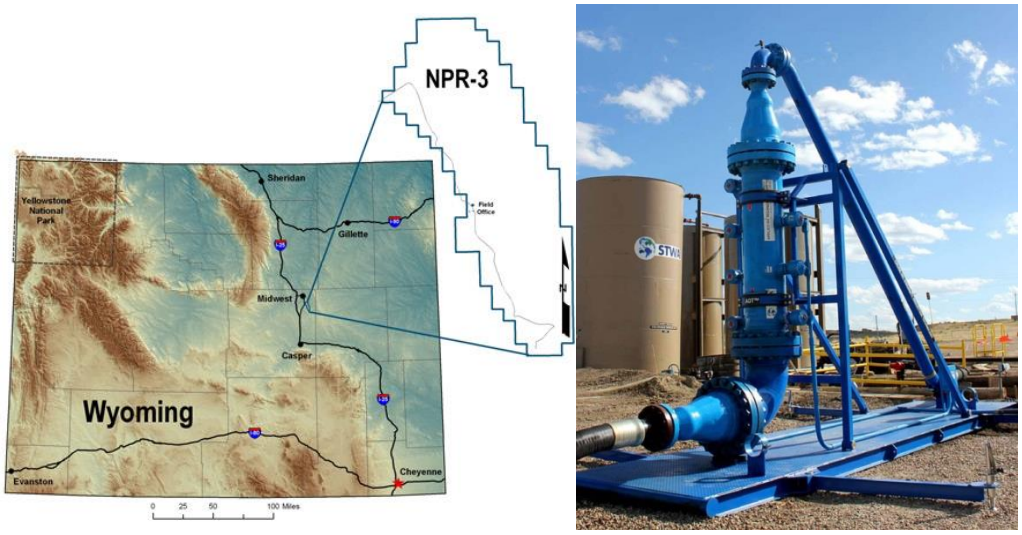

Fig. 5.7 The DOE pipeline test location and set up

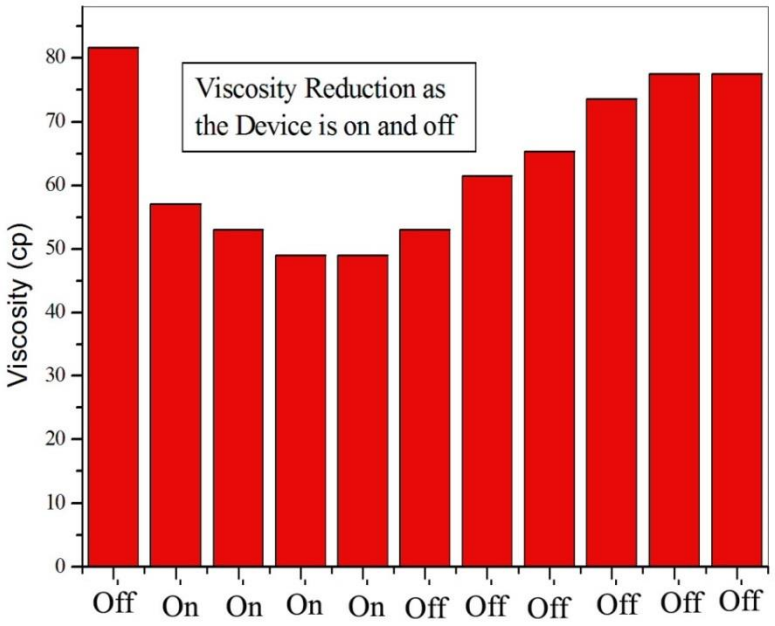

Fig. 5.8 Viscosity reduction as the device is turned on and off

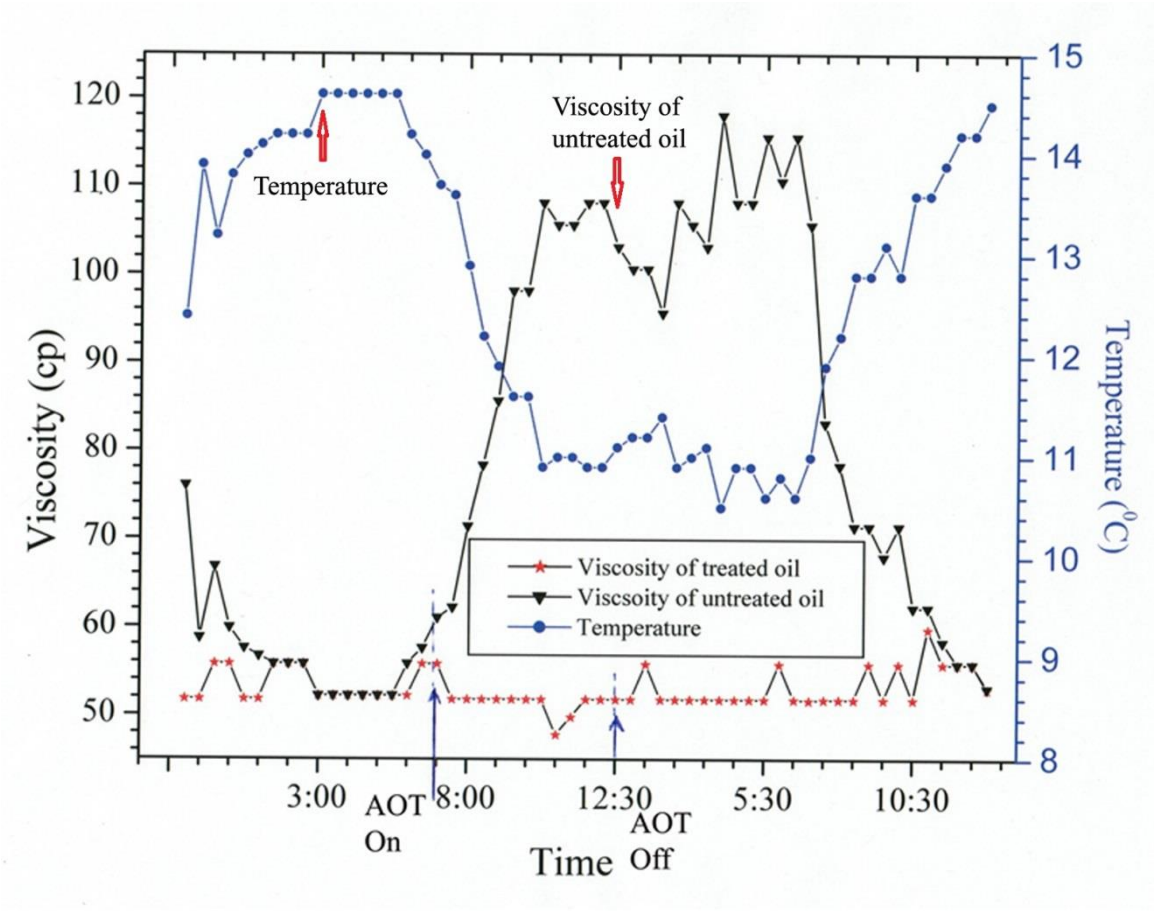

Fig. 5.9 The crude oil keeps the reduced viscosity for 11 hours as it flows inside the pipeline.

5.3 Daqing Oil Field Pipeline Testing [12].

At the Daqing field, which is the largest oil field in the People's Republic of China, the crude oil has pour point 33^0C, The oil is heated at one station and flows 14km to next heating station.

Fig. 5.10 Tests at Daqing oil field in China.

E-Field (kV/cm)	T (^{0}C)	Vis (cSt)	Pressure (bar)	Flow rate (m^3/h)
0	55.6	20.36	3.1	16.4
16	55.6	17.02	3.1	19.6
16	55.6	17.02	7.0	44.6

Table. 5.1 Test results at Daqing oil field in China.

5.4 Wichita Keystone Pipeline Testing

The keystone pipeline is the main pipeline to carry Canadian crude oil to US refineries in Texas and Illinois. [13-16]

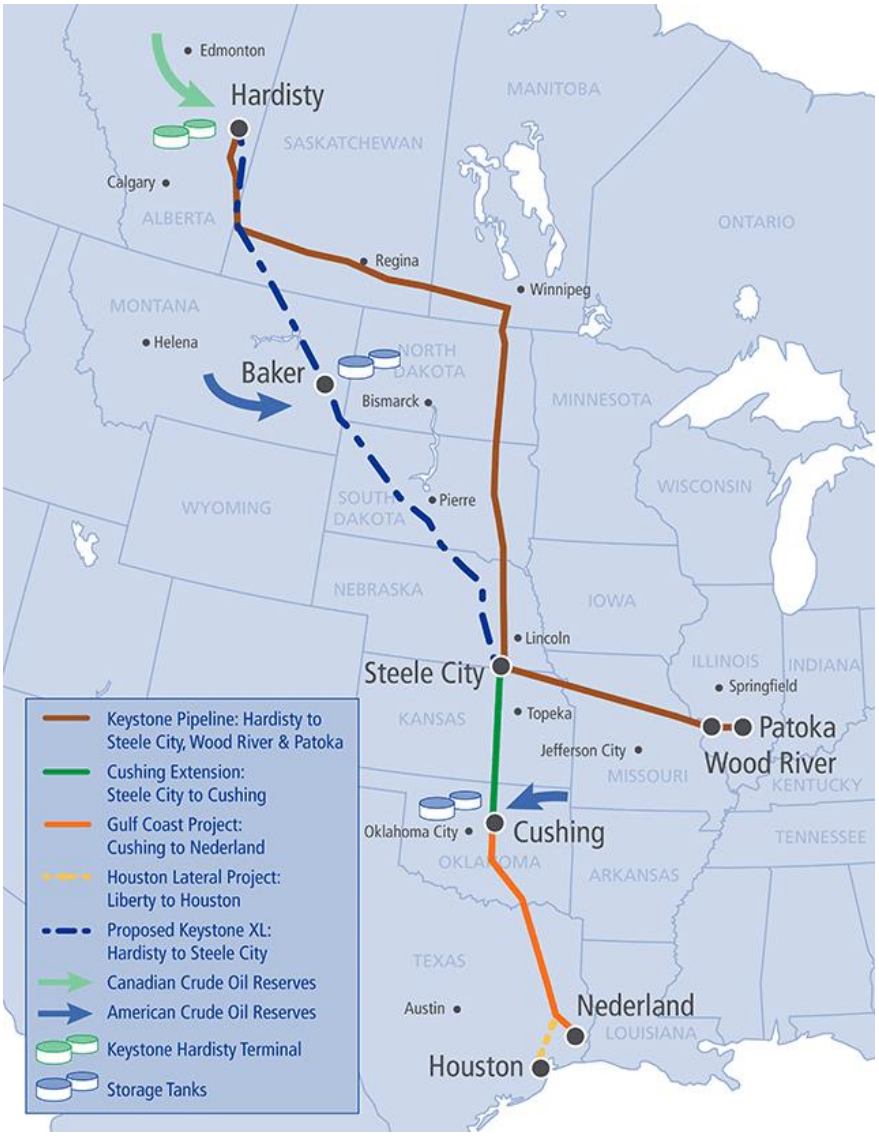

Fig. 5.11 Keystone pipeline

TransCanada decided to hire Inspectorate USA as an independent company to verify the test results at next test. On 9/16/2014, at the second test, two independent companies, Inspectorate USA and Cannon Instrument Company were hired to verify the test results. Both companies have confirmed the test results.

Fig. 5.12 Our Device on Keystone Pipeline near Wichita,Kansas,

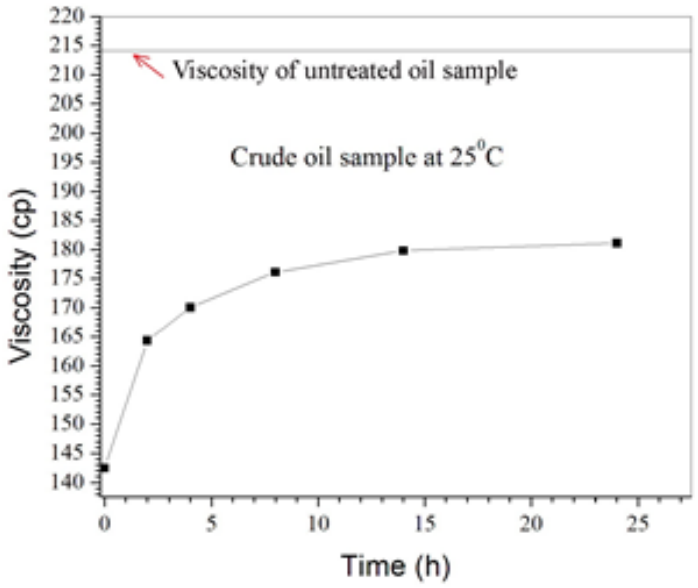

Fig. 5.13 Keystone Pipeline tested viscosity with time

The crude oil originally had viscosity 210.1cp at 25^{0}C. Application of the electric field reduced it to 142.5cp. It then slowly increased.

E-Field (kV/cm)	T (^{0}C)	Viscosity (cp)	Flow rate (m^3/h)	Renolds #	Pump Power (kW)
0	25	214.1	2280	3758	2826
1.44	25	142.5	2280	5646	Reducing to 790 kW

Table. 5.2 energy saved by e_filed

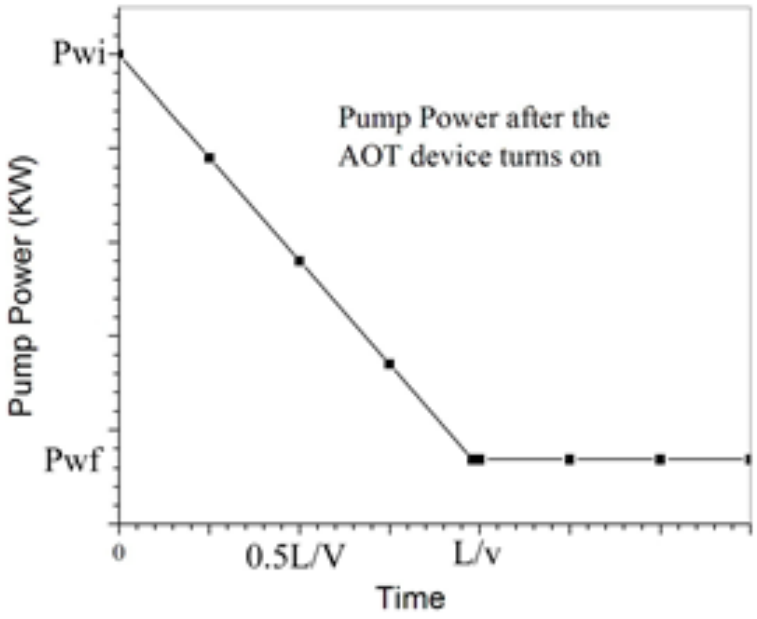

Fig. 5.14 The pump power dropped with our device on

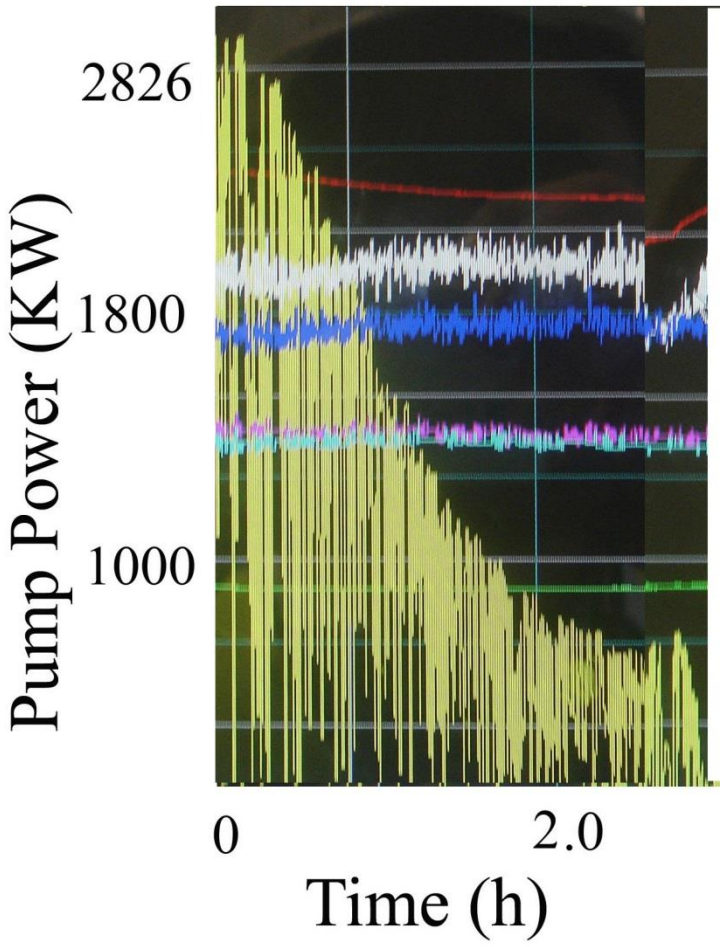

Fig. 5.15 The pump power was significantly reduced from 2.8MW to 1.8MW with our device on

Once the device was turned on, the pump power was significantly reduced from 2.8MW to 1.8MW. Then, the flow rate dropped due to an upstream pump switch. However, after that, the pump power continued to drop.

Application of electrorheology breaks the rotational symmetry and makes the viscosity anisotropic. It reduces the viscosity along the pipeline and increase the flow rate. At the same time, it increases the viscosity in the direction perpendicular to the flow

direction. This suppresses the turbulence. The technology has huge applications in energy production.

References

[1]Tao R. & Xu X. Reducing the viscosity of crude oil by pulsed electric or magnetic field. Energy & Fuels 2006; 20**:** 2046-2051.

[2]Tao R. Electrorheology for efficient energy production and conservation. J. of Intelligent Material Systems and Structures 2011: 22**:** 1667-1671.

[3]Tang H., Huang K. & Tao R. Electrorheology improves transportation of crude oil. J. of Intelligent Material Systems and Structures 2011; **22:** 1673-1676.

[4] Du, E., Tang, H., Huang, K. and Tao, R., Reducing the viscosity of diesel fuel with electrorehological effect, Journal of Intelligent Material Systems and Structures.53, 59 (2011)

[5] Huang, K., Du, E., Tang, H. and Tao, R., Electrorheology improves E85-engine performance and efficiency, Journal of Intelligent Material Systems and Structures. 60,67 (2011)

[6] R. Tao and G. Q. Gu, Suppressing turbulence and enhancing liquid suspension flow in pipelines with electrorheology, Phys. Rev. E 91, 012304 (2015)

[7] Tao, R.; Du, E.; Tang, H.; Xu, X., Neutron scattering studies of crude oil viscosity reduction with electric field, Fuel, 134, 493,498 (2014)

[8] report of Petro China Pipeline P&D Center，
http://content.stockpr.com/stwa/media/da44e1432e71850cfbf79b5f1fed1ceb.pdf

[9] Successfully Completes Lab Testing AOT in China & Schedules Field Test for August http://www.stwa.com/news/detail/1643/commercial-pipeline-field-testing-in-china-confirms

[10] U.S. Department of Energy's (DOE) Rocky Mountain Oilfield Testing Center (RMOTC) http://www.stwa.com/news/detail/453/stwa-inc-provides-update-on-timeline-for-aot-testing

[11] Phase II testing with the U.S. Department of Energy
http://www.stwa.com/news/detail/353/stwa-issues-phase-ii-testing-update-on-applied-oil

[12]AOT 1.3vx Completes Phase II Testing on Active Commercial Pipeline Located on the Daqing Oilfield in Northeastern China
http://www.stwa.com/news/detail/1643/commercial-pipeline-field-testing-in-china-confirms

[13]TransCanada Tries A New Clean-Tech Pipeline Solution
http://seekingalpha.com/article/2135793-transcanada-tries-a-new-clean-tech-pipeline-solution

[14] Electric Field Would Improve Flow in Keystone Pipeline
http://spectrum.ieee.org/energywise/energy/fossil-fuels/electric-field-would-improve-flow-in-keystone-pipeline

[15] Saving energy: Increasing oil flow in the Keystone pipeline with electric fields
http://www.sciencedaily.com/releases/2015/02/150227112751.htm

[16] Saving energy: Increasing oil flow in the Keystone pipeline with electric fields
http://www.eurekalert.org/pub_releases/2015-02/aps-sei022715.php

CHAPTER 6

RESULT ANALYSIS AND CONCLUSION

6.1 Neutron Scattering Amplitude Calculation

The Hamiltonian for the neutron particles is $H = -\hbar^2\nabla^2/(2m) + V$, where V is the neutron-nuclear interaction, responsible for the neutron scattering. For our tests, the first Born approximation provides excellent description of the neutron wave function[16-18], $\Psi(\vec{r}) = \exp(i\vec{k_i}\cdot\vec{r}) + \frac{\exp(ik_s r)}{r} f(\theta)$. The scattering amplitude is given by

$$f(\theta) = (\frac{m}{2\pi\hbar^2})\int d\vec{r}\,'\exp(-i\vec{Q}\cdot\vec{r}\,')V(\vec{r}\,'). \qquad (6.1)$$

$\vec{Q} = \vec{k}_s - \vec{k}_i$ is the scattering vector. For our elastic scattering, $k_i = k_s = 2\pi/\lambda$ and $\lambda = 6\,\mathring{\mathrm{A}}$. The scattered intensity is proportion to the scattering cross section, $I(\vec{Q}) \propto \frac{d\sigma(\vec{Q})}{d\Omega} = |f(\theta)|^2$. As the neutron-nuclear interactions are short ranged, the Fermi-pseudo potential is suitable, $V(\vec{r}) = (\frac{2\pi\hbar^2}{m})\sum_j^N b_j\delta(\vec{r}-\vec{r}_j)$. Hence, $f(\theta) = \sum_j^N b_j \exp(-i\vec{Q}\cdot\vec{r}_j)$. We define a scattering length density, $\rho(\vec{r}) = \sum_j^N b_j\delta(\vec{r}-\vec{r}_j)$, then we have

$$I(\vec{Q}) \propto \frac{1}{V}|\int_V d\vec{r}\,\rho(\vec{r})\exp(i\vec{Q}\cdot\vec{r})|^2 \qquad (6.2)$$

Following the standard approach for dilute systems, we denote the scattering length density by the base liquid as ρ_0 and the scattering length density by the particles as ρ_p. Thus $\rho(\vec{r}) = \rho_p$ in the volume occupied by the particles, V_p, and $\rho(\vec{r}) = \rho_0$ in the volume occupied by the base liquid. Typically, $\rho_p > \rho_0$. Then equation (6.2) becomes

$$I(\vec{Q}) \propto \frac{1}{V}(\rho_p - \rho_0)^2 |\int_{V_p} d\vec{r}\exp(i\vec{Q}\cdot\vec{r})|^2, \qquad (6.3)$$

where the integration only takes over the volume occupied by the particles. Here

$$\int_{v_p} d\vec{r} \exp(i\vec{Q}\cdot\vec{r}) = F(\vec{Q}) \tag{6.4}$$

is the form factor and $I(\vec{Q}) \propto |F(\vec{Q})|^2$.

The main goal of my thesis research was to study the aggregation of particles in crude oil into viscosity reducing chains using neutron scattering. As shown in Fig. 6.1, without the electric field applied, the neutrons are scattered into all directions, indicating that the suspended particles are randomly distributed inside the crude oil. However, as shown in Fig. 6.2-6.5, when a strong electric field is applied, the scattering patterns changed: they became elliptic with the long axis perpendicular to the electric field direction and the patterns became more and more solid. All these indicate that after a strong electric field is applied, the particles aggregate into ellipsoid chain along the field direction. This aggregation changes $I(\vec{Q})$. Especially when the electric field is above 400V/mm, the scattered patterns indicate that the particles inside the aggregated chains are closely packed.

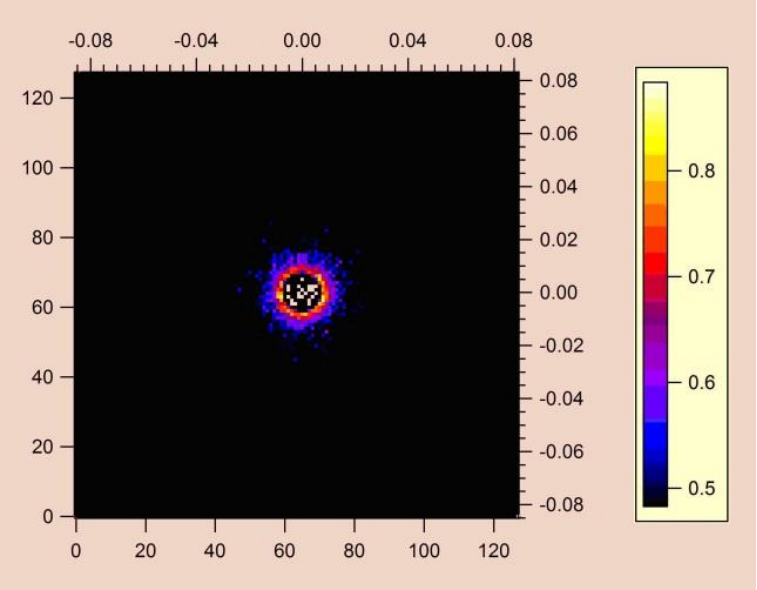

Fig. 6.1 The neutron scattering pattern without electric field applied

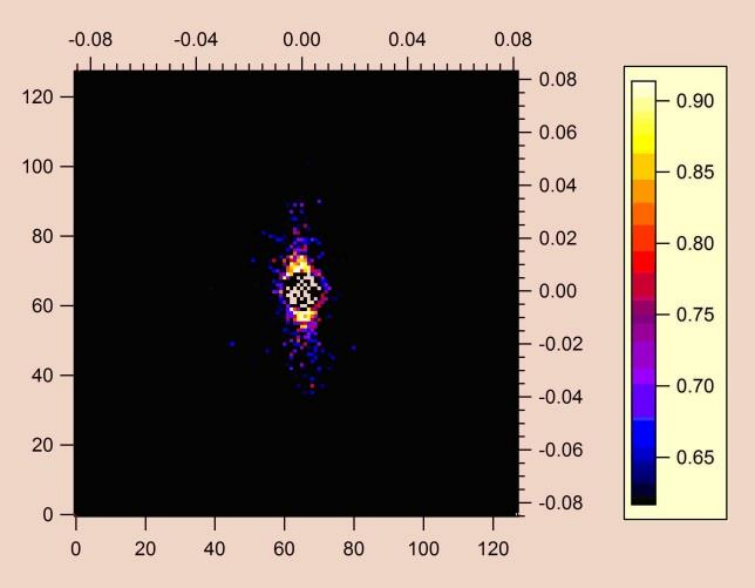

Fig. 6.2 The neutron scattering pattern with electric field applied E=250V/mm

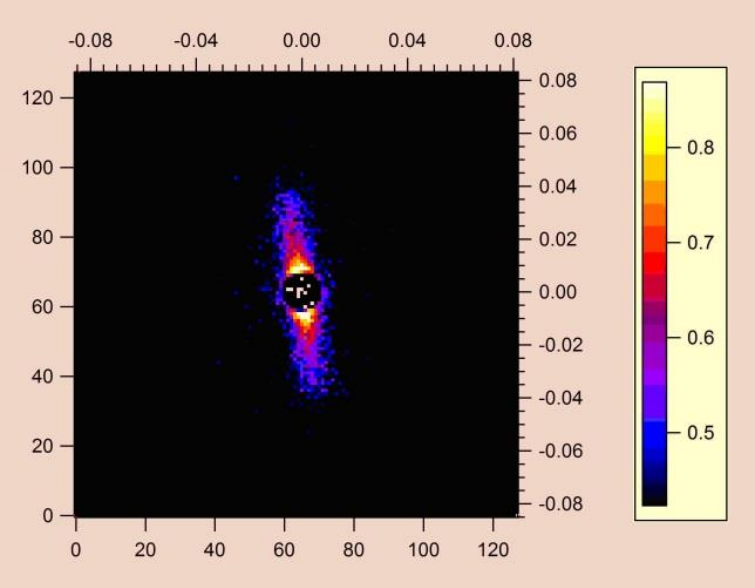

Fig. 6.3 The neutron scattering pattern with electric field applied E=400V/mm

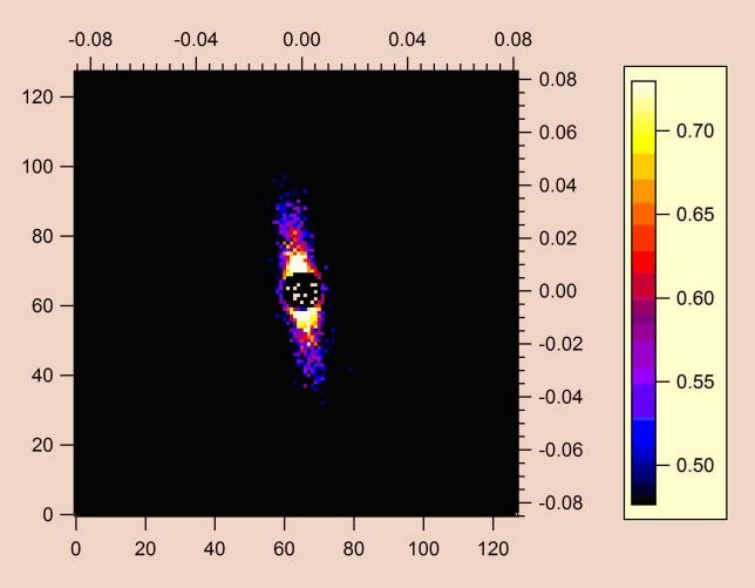

Fig. 6.4 The neutron scattering pattern with electric field applied E=750V/mm

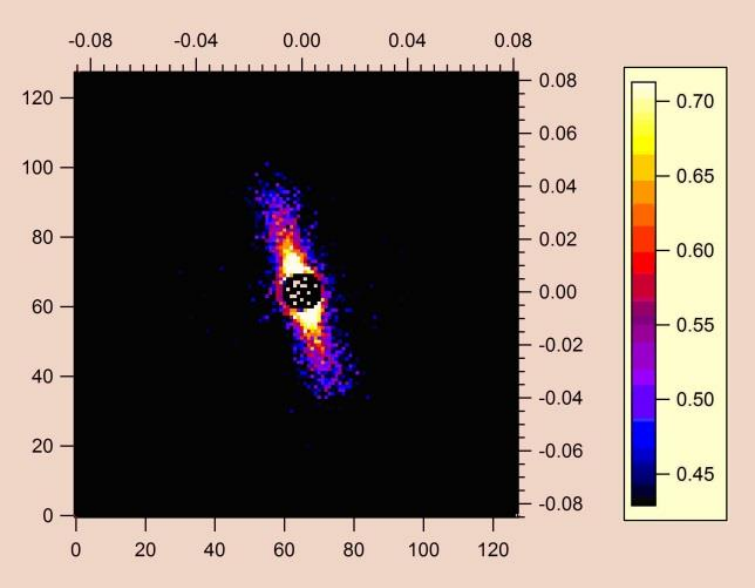

Fig. 6.5 The neutron scattering pattern with electric field applied E=1100V/mm

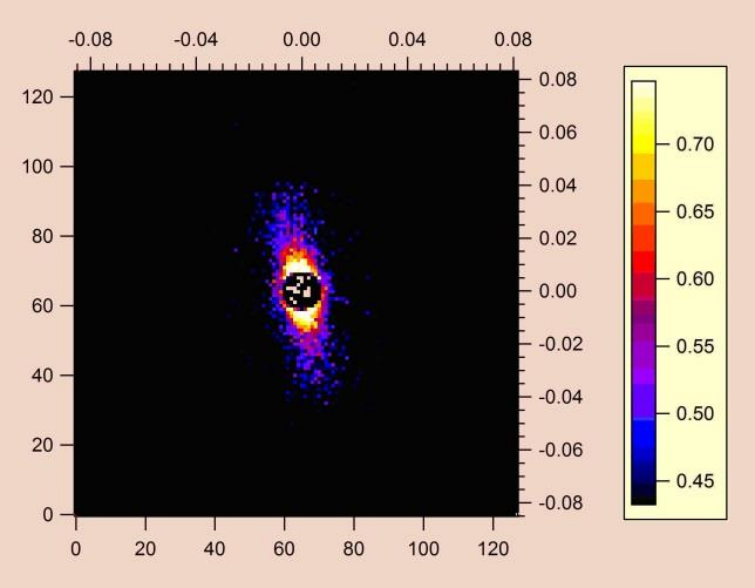

Fig. 6.6 The neutron scattering pattern with electric field applied E=1500V/mm

6.2 The Guinier Approximation

Let the electric field be along the x-direction and incoming neutron beam in the z-direction. From the scattering signal, we assume that the aggregated chain or chain-based column can be approximated as a prolate spheroid with its rotational axis along the field direction,

$$x^2 / a^2 + (y^2 + z^2) / b^2 = 1 \tag{6.5}$$

where $a > b$. Similar to Guinier,[18-19], we define a function,

$$\Phi(t) = 3 \cdot [\sin(t) - t\cos(t)] / t^3 \tag{6.6}$$

The form factor of the spheroid in Eq.(6.5) is $(4\pi ab^2 / 3)\Phi(\sqrt{(aQ_x)^2 + b^2(Q_y^2 + Q_z^2)})$ and the scattering intensity is given by

$$I(\vec{Q}) = I_0 \,|\, \Phi(\sqrt{(aQ_x)^2 + b^2(Q_y^2 + Q_z^2)}) \,|^2 \tag{6.7}$$

In our experiment, $Q_z = 0$ as $\vec{Q}$ is perpendicular to the direction of the incoming beam. The function $|\Phi(t)|^2$ has its maximum 1 at $t = 0$ and is decreasing as *t* increases. From Eq. (6.7), at the center $\vec{Q} = 0$, the maximum scattering intensity is I_0, which equals to 3.0, indicating that 3000 neutrons were detected along the $\vec{Q} = 0$ direction. Because of the beam stop issue, in all scattering patterns (Fig,6.1-Fig.6.6) the area near $\vec{Q} = 0$ is blacked out. Fortunately, $|\Phi(t)|^2$ initially decreases quite slowly until $t \le 0.7$; therefore, this issue does not create any difficulty for our data analysis. As $\sqrt{(aQ_x)^2 + (bQ_y)^2}$ further increases, the scattering intensity rapidly decreases. For example, along the elliptic curve, $(Q_x a / 2.6677)^2 + (Q_y b / 2.6677)^2 = 1$, the scattering intensity is reduced to $0.2I_0$ and similarly along the elliptic curve, $(Q_x a / 2.498)^2 + (Q_y b / 2.498)^2 = 1$, the scattering intensity is $0.25I_0$. As shown in Figures 3 and 4, the scattering intensity is denoted by colors. Hence, from the scattering intensity pattern, we can derive *a* and *b* and determine the size and shape of the aggregated chains.

With the above analysis, it is clear that when the applied electric field is 250V/mm (Fig. 6.2), the particles begin to aggregate into short chains, which have length $2a = 68nm$ and thickness $2b = 34nm$. As the electric field is increased to 400V/mm (Fig. 6.3), the chain are 75.2nm long and 37.6nm thick. When E=750V/mm (Fig. 6.4), the chain is 94nm long and 38.4nm thick. With the electric field of 1100V/mm (Fig. 6.5), the chain is 74.8nm long and 38.6nm thick. Finally, at E=1500V/mm (Fig. 6.6), the chain has 74.8nm length and 45nm thickness. It is clear that as the electric field increases, the aggregated chains become longer and thicker (Table 6.1).

The aggregation of suspended particles is the result of induced dipolar interaction. Therefore, the aggregated chains are parallel to the electric field direction. The elliptic shapes of our scattering patterns indicate that the effective electric field in our capacitor is slightly tilted from horizontal.

6.3 Intrinsic Viscosity Of The Aggregated Particles

The neutron scattering experiment reveals that the aggregated chains are similar to prolate spheroids with the long rotational axis along the field direction. For such spheroids, the intrinsic viscosity along the field direction is smaller than 2.5, the intrinsic viscosity for spheres.[20] For example, at E=750V/mm, we have $(a-b)/a = 0.5915$ and the intrinsic viscosity $\nu = 2.125$ along the long the field direction. The intrinsic viscosity for various electric fields is listed in Table 1.

The Krieger-Dougherty equation[21] enables us to estimate the effective viscosity,

$$\eta_{eff} / \eta_0 = (1 - \phi / \phi_{\max})^{-\nu\phi_{\max}} \qquad (6.8)$$

where η_0 is the viscosity of base liquid, ν the intrinsic viscosity, and $\phi_{\max}$ the maximum volume fraction for randomly packing the particles. When there is no electric field applied, the suspended particles are spherical, $\phi_{sphere} = 0.64$ and $\nu = 2.5$, and the crude oil has viscosity $\eta_{eff} = 11.38\eta_0$ for volume fraction $\phi = 0.5$. After an electric field of 1100V/mm applied, the intrinsic viscosity of the aggregated particles along the field direction is reduced to 2.124 and the maximum random packing fraction for spheroids $\phi_{spheroid}$ is increased to 0.72.[22-23] Then the effective viscosity along the field direction is $6.129\eta_0$. The viscosity along the field direction is reduced by 46.14%. As shown in Fig.1, in our technology application, the applied electric field is parallel to the flow direction. Therefore, the oil flow is greatly improved once the electric field is applied. This is consistent with our lab tests and field tests.[5-7]

A comparison of the intrinsic viscosities at various electric fields in Table 6.1 indicates that as the applied electric field increases, the length of the aggregated chains

increases rapidly, quickly lowering the intrinsic viscosity. However, after the electric field reaches 1100V/mm, a further increase of the electric field mainly makes the chains thicker, leading to a higher intrinsic viscosity. Therefore, it is clear that there is an optimal electric field for the viscosity reduction, and it is not true that the higher the electric field, the greater the viscosity reduction.

As shown in Fig. 6.4, the electric field treatment also works well with asphalt base crude oil. Similar to paraffin base crude oil, a strong electric field aggregates the suspended asphalt particles inside our heavy asphalt crude oil sample, APT 21, into short chains along the field direction. Further more, as the electric field can reduce the viscosity for both paraffin base crude oil and asphalt base crude oil, it is certain that the electric field can also reduce the viscosity of mixed base crude oil. Therefore, electric field is universal, effective in reducing the viscosity of all kinds of crude oils.

In summary**, t**he neutron scattering experiment has resolved the controversy and unambiguously confirmed that a strong electric field aggregates the suspended nano-particles inside crude oil into short chains along the field direction, reducing the effective viscosity along the field direction significantly. The electric field works for all kinds of crude oils. The underlying physics demonstrated by this neutron scattering experiment is applicable to all kinds of suspensions, and one expects many practical applications.

References

[1]Tao R. & Xu X. Reducing the viscosity of crude oil by pulsed electric or magnetic field. Energy & Fuels 2006; 20: 2046-2051.

[2]Tao R. Electrorheology for efficient energy production and conservation. J. of Intelligent Material Systems and Structures 2011: 22: 1667-1671.

[3]Tang H., Huang K. & Tao R. Electrorheology improves transportation of crude oil. J. of Intelligent Material Systems and Structures 2011; 22: 1673-1676.

[4]For example, see *Science News (Oct.28, 2006, V170 #18), New Scientist (Aug. 29, 2006), Oil&Gas (issue 7,pp37-38, 2011), GeoTime (Nov. 2006), Chemistry-Industry(Sept. 18, 2006), Philadelphia Inquirer (Sept 29, 2006).*

[5] www.rmotc.doe.gov/PDFs/STWA%20Test%20Report%20-%20Final%20May%202012.pdf

[6] www.rmotc.doe.gov/PDFs/STWA%20Test%20Report%20-%20FINAL.pdf

[7] www.rmotc.doe.gov/PDFs/TS19_51141_Final%20Report.pdf

[8] Miesowicz M. The three coefficients of viscosity of anisotropic liquids. *Nature* 1946; 158: 27.

[9] Evdokimov I. N. & Kornishin K. A. Apparent Disaggregation of Colloids in Magneticalls Treated Crude Oil, *Energy & Fuel* 2009, 23, 4016-4020.

[10] Tao R. & Sun J. Three-dimensional Structure of Induced Electrorheological Solid, *Phys. Rev. Lett*. 1991, V67, 398-401.

[11] Chen T. J., Zitter R. N. & Tao R. Laser Diffraction Determination of the Crystalline Structure of an Electrorheological Fluid, *Phys. Rev. Lett* 1992, V68, 2555-2558.

[12] Tao R. & Jiang Q. Simulation of Structure Formation in an Electrorheological Fluid, Phys. Rev. Lett. 1994, V73, 205-208 .

[13] K. Agarwai & A. Yethiraj, Phys. Rev. Lett. 102, 198301:1-4 (2009).

[14] Tao R.& Huang K. Reducing blood viscosity with magnetic fields, *Phys. Rev. E* 2011, 84, 011905: 1-5.

[15] Goncalves J.L. et al. Study of the factors responsible for the rheology change of a brazilian crude oil under magnetic fields. Energy & Fuels 2011; 25: 3537-3543

[16] Glinka, C.J. et al. The 30 m small-angle neutron scattering instruments at the national institute of standards and technology. *J. Appl. Cryst* 1998, 31, 430-445.

[17] Squires G. L. Introduction to the Theory of Thermal Neutron Scattering. Dover Publications (1978).

[18] Pedersen, J.S. Analysis of small angle scattering date from colloids and polymer solutions: modeling and least-squares fitting. Advances in Colloid and Interface Science 1977, 70, 171-210.

[19]Guinier, A. Diffraction of X-rays of very small angles – application to the study of ultramicroscopic phenomena. *Ann. Phys*. (Paris) 1939, 12, *161–237*

[20] Jefferry G. B. The Motion of Ellipsoidal Particles Immersed in a Viscous Fluid, Proceedings of the Royal Society of London Series A 1922, V.102, 161-179.

[21] Krieger I. M. & Dougherty T. J. A Mechanism for Non-newtonian Flow in Suspensions of Rigid Spheres. Tans. Soc. Rheol. 1959; 3: 137-152.

[22] Donev, A. *et al*, Improving the Density of Jammed Disordered Packings Using Ellipsoids, *Science* 2004, 303, 990-993.

[23] Man, W. *et al*, Experiments on Random Packings of Ellipsoids, *Phys Rev Lett* 2005, 94, 198001 1-4.

[24] Tao R. & Tang H. Reducing viscosity of paraffin base crude oil with electric field for oil production and transportation, *Fuel* 2014, V.118, 69-72.

[25] Du, E., Tang, H., Huang, K. and Tao, R., Reducing the viscosity of diesel fuel with electrorehological effect, Journal of Intelligent Material Systems and Structures.53, 59 (2011)

[26] Huang, K., Du, E., Tang, H. and Tao, R., Electrorheology improves E85-engine performance and efficiency, Journal of Intelligent Material Systems and Structures. 60,67 (2011)

[27] R. Tao and G. Q. Gu, Suppressing turbulence and enhancing liquid suspension flow in pipelines with electrorheology, Phys. Rev. E 91, 012304 (2015)

[28] Tao, R.; Du, E.; Tang, H.; Xu, X., Neutron scattering studies of crude oil viscosity reduction with electric field, Fuel, 134, 493,498 (2014)